RORc expressing immune cells support pro-tumorigenic functions of tertiary lymphoid structures

Einat Cinnamon[1], Ilan Stein[1,2], Elvira Zino[1], Stav Rabinovich[1], Yehuda Shovman[1], Yehuda Schlesinger[1], Tomer-Meir Salame[3], Shlomit Reich-Zeliger[4], Michal Lotem[5], Yinon Ben-Neriah[1], Oren Parnas[1] and Eli Pikarsky[1,2*]

Affiliations:

[1]The Concern Foundation Laboratories at The Lautenberg Center for Immunology and Cancer Research, Israel-Canada Medical Research Institute, Faculty of Medicine, The Hebrew University, Jerusalem, Israel

[2]Department of Pathology, Hadassah-Hebrew University Medical Center, Jerusalem, Israel

[3]Flow Cytometry Unit, Life Sciences Core Facilities, Weizmann Institute of Science, Rehovot, Israel

[4]Department of System Immunology, Weizmann Institute of Science, Rehovot, Israel

[5]Sharett Institute of Oncology, Hadassah-Hebrew University Medical Center, Jerusalem, Israel

*corresponding author: peli@hadassah.org.il

Abstract:

Tertiary lymphoid structures (TLSs) are formed in many cancer types and have been correlated with better prognosis and response to immunotherapy. In liver cancer, TLSs have been reported to be pro-tumorigenic as they harbor tumor progenitor cells and nurture their growth. The processes involved in TLS development and acquisition of pro- or anti-tumorigenic phenotype in cancer are largely unknown. RORc expressing immune cells have been previously implicated in TLS formation, however we find that they are not necessary for TLS neogenesis in the liver under chronic inflammation conditions. On the contrary, RORc expressing cells rather negatively regulate TLS formation, since in their absence TLSs form in excess. Importantly, in chronically inflamed livers lacking RORc expressing cells, pro-tumorigenic TLSs become anti-tumorigenic, resulting in reduction of tumor load. Comparing liver pro- and anti-tumorigenic TLSs by transcriptional, proteomic and immunohistochemical analyses, revealed an enrichment of exhausted CD8 cells that

retained effector functions and had a progenitor-like proliferative phenotype in anti-tumorigenic TLSs. Similar observations were found when comparing pro- and anti-tumorigenic TLSs in human tissues. Thus, RORc expressing cells negatively regulate CD8 cell abundance, and facilitate the pro-tumorigenic functions of hepatic TLSs.

Introduction:

Tertiary lymphoid structures (TLS) are aggregates of immune cells that form in nonlymphoid tissues in response to chronic inflammation, autoimmunity and cancer. In cancer, TLSs have been described in many tumor types such as non–small cell lung cancer (NSCLC), colorectal cancer (CRC), ovarian cancer and melanoma. TLS density has been correlated with better patient survival in many cancer types and it has been suggested that TLSs contribute to the strength of tumor specific immune response (Schumacher & Thommen, 2022)(Sautès-Fridman et al., 2019). Yet, a pro-tumorigenic role for TLSs in the context of liver cancer was recently described in human and mice (Finkin et al., 2015). Using a mouse model mimicking chronic liver inflammation (by overactivation of the NF-κB pathway in hepatocytes), the development of liver TLSs, harboring liver cancer progenitor cells that egress out of the TLSs and form nearby tumors, was demonstrated. TLS and tumor formation were dependent on an intact adaptive immune system since in Rag1$^{-/-}$ mice both TLS and tumor formation was abrogated. Moreover, TLS derived Lymphotoxin (LT)β promoted cancer progenitor growth (Finkin et al., 2015). Indeed, several other studies have shown that TLSs can be pro-tumorigenic: in breast cancer TLSs are associated with more aggressive tumors (Figenschau et al., 2015) and Tregs in lung cancer TLSs can inhibit endogenous immune responses against tumors (Joshi et al., 2015). Interestingly, while our analysis revealed that TLSs in the inflamed liver parenchyma are associated with a bad prognosis in human hepatocellular carcinoma (HCC), a later study reported that intratumor TLSs in the liver are associated with good prognosis (Calderaro et al., 2019). Yet the same group later reported that in early HCCs, TLSs show pro-tumorigenic functions (Meylan et al., 2020). Intrahepatic cholangiocarcinoma (iCCA) is the second-most common primary liver malignancy after HCC. Current available therapies for iCCA have limited efficacy, and surgery remains the only curative option, despite the extremely high postoperative recurrence rate (Bertuccio et al., 2019). Recent findings show that TLSs in intratumor regions of iCCA were correlated with a favorable prognosis while

peri-tumoral TLSs signified worse survival (Ding et al., 2022). Thus, understanding TLS neogenesis and the acquisition of TLS phenotypes that influence their functions could have important implications for immunological treatments in some cancer types.

TLS formation was compared to the formation of secondary lymphoid organs (SLO), such as lymph nodes developing during embryogenesis, and involves interaction between hematopoietic cells and nonlymphoid stromal cells. SLO formation is initiated by the colonization of the lymph node anlagen by hematopoietic lymphoid tissue inducer (LTi) cells which in this case are $CD4^+$ $CD3^-$ $CD45^+$ innate lymphoid cells, characterized by the expression of the RORγt (the shorter isoform of RORγ, also called RORc) and Id2 transcription factors. LTα1β2 and tumor necrosis factor (TNF), secreted by LTi cells, bind to their receptors on mesenchymal lymphoid tissue organizer (LTo) cells and drive the expression of adhesion molecules and cytokines that recruit immune cells to the lymphoid niche. Accordingly, LTi cells depend on RORc expression for their formation and RORc knockout mice lack SLOs (Schumacher & Thommen, 2022).

Although the formation of TLSs and SLOs was initially thought to be induced by the same molecular factors, the cellular components involved are at least partially different (Schumacher & Thommen, 2022) and many aspects of this process are only partly understood. Our understanding of the cellular and molecular processes that drive TLS formation has been obtained mainly in models of autoimmunity and chronic infection, and therefore their relevance to TLS formation in cancer remains to be determined. For instance, TLSs in the adult gut, termed ILFs, were shown to depend on RORc expressing LTi cells for their formation (Tsuji et al., 2008). However, TLSs can also form independently of LTi cells since they are present in RORc- and Id2-deficient mice in the context of inflammation and autoimmunity (Lochner et al., 2011)(Rangel-Moreno et al., 2011)(Marinkovic et al., 2006). Other cell types have been shown to function as LTi cells during TLS formation, such as Th17 in neuroinflammation (Pikor et al., 2015), B cells in intestinal inflammation (Lochner et al., 2011), and mature $CD3^+CD4^+$ cells in the thyroid (Marinkovic et al., 2006). Little is known about the cell types involved in TLS neogenesis in the context of cancer. In lung cancer, NCR^+ innate lymphoid cell (ILC)-3s have been shown to have LTi properties and might contribute to the formation of TLSs (Carrega et al., 2015). In lung cancer and melanoma murine models, effector $CD8^+$ T cells and natural killer (NK) cells were shown to induce lymph-node like vasculature which correlates

with TLS formation (Peske et al., 2015). In a murine melanoma model, CD8 cells were found to act as LTi cells by organizing cancer associated fibroblasts into a reticular network (Rodriguez et al., 2021). Thus, the requirement of LTi-like cells for TLS neogenesis in cancer remains largely unknown.

RORc is a nuclear hormone receptor which is necessary for T helper 17 (Th17) cells differentiation, innate lymphoid cell (LTi and ILC3) development and functions of γδ T cells. Mice that lack RORc expression do not develop these cell types, some of which have been implicated in TLS neogenesis, and fail to develop lymph nodes or Peyer's patches. We asked whether RORc expressing cells are required for TLS neogenesis in the liver under chronic inflammation conditions which result in liver cancer. We find that although RORc expressing cells are found in TLSs, they are dispensable for their neogenesis. Surprisingly, we find that in the absence of RORc$^+$ cells, TLSs form in excess, suggesting they negatively regulate TLS formation. Importantly, TLSs forming in the absence of RORc are no longer pro-tumorigenic and show reduced formation of TLS-derived liver tumors. Phenotyping liver immune cells in the absence of RORc$^+$ cells, at the transcriptomic and protein levels, identified an increase in CD8 cells with a mixed exhausted/effector phenotype, as well as an increase in resident memory cells and shift from pro-tumorigenic T helper (T_{H2}) to an anti-tumorigenic T helper (T_{H1}) phenotype of CD4 cells. Anti-tumorigenic TLSs showed enrichment in CD8 cells with a progenitor like proliferative state compared to pro-tumorigenic TLSs. Our results suggest that RORc expressing cells negatively regulate CD8 cells required for tumor surveillance. In conclusion, we show that RORc$^+$ cells have multiple roles in TLS driven liver cancer, first by negatively regulating TLS neogenesis and second by contributing to TLSs promotion of liver cancer formation.

Methods:

Reagent type	**Designation**	**Source**	**Identifier**	**Additional information**
Tissue Digestion	Accumax	Sigma	A7089	1 : 2
Tissue Digestion	Liver digest medium	GIBCO	17703-034	used at 100%
Enzyme	Deoxyribonuclease I from bovine pancreas (DNAse)	Sigma/Merck	DN25	0.07%
DNA stains	Propidium Iodide solution	CliniSciences	30901000-1	1 : 500

DNA stains	Trypan blue	Sigma	T8154	1 : 2
DNA stains	Hematoxilyn	Kaltek Srl	1100	
Chemical	Percoll	Sigma	P1644-500ML	
Chemical	Diethylnitrosamine (DEN)	Sigma	N0258	10 mg/kg
Chemical	Foxp3 / Transcription Factor Staining Buffer Set	eBioscience	00-5523-00	
inhibitor	Brefeldin A	Biolegend	420601	
Serum	Donkey serum	Merck	D9663	
Serum	Rat Serum	Merck	R9759	1 : 100
Serum	Fetal Bovine serum	Biological Industries	04-007-1A	
Serum	BSA	Sigma	A3803	
Antibody	PB-conjugated-anti-CD45	Biolegend	109820	1 : 500
Antibody	APC-conjugated-anti-F4/80	eBioscience	17-4801-82	1 : 50
Antibody	CD16/CD32 Monoclonal Antibody (93) (Fc Blocker)	eBioscience Invitrogen	14-0161-82	1 : 100
Antibody	anti-Sox9	Millipore	AB5535	1 : 1000, Citrate
Antibody	anti-E-cadherin	Transduction Laboratories	610181	1 : 200, Citrate
Antibody	anti-CD44v6	eBioscience	BMS145	1 : 500, Citrate
Antibody	anti-HNF4a	Abcam	ab201460	1 : 2000, Tris
Antibody	anti-CK19	DSHB	TROMA-III CK19	1 : 25, Citrate
Antibody	anti- mouse CD8	Invitrogen	14-0808-80	1 : 50 , Citrate
Antibody	anti-CD4	Invitrogen	14-9766-80	1 : 50 , Citrate
Antibody	anti-mouse PD1	R&D systems	AF1021	1 : 100, Citrate
Antibody	anti-mouse/human Ki67	Abcam	ab15580	1 : 200,
Antibody	anti-Foxp3	eBioscience	14-5773	1 : 50,
Antibody	anti-RORc	Abcam	ab207082	1 : 1000, TRIS
Antibody	anti-Tcf1/7	Cell Signaling	2203	1 : 100, Citrate
Antibody	anti-Ly6G	BD pharmingen	551459	1 : 250, Citrate
Antibody	anti-human PD1	Cell Marque	315M-95	1 : 100
Antibody	anti-human CD8	Abcam	ab101500	1 : 50
Antibody	HRP-conjugated anti-Rat	Histofine	11-414311F	
Antibody	HRP-conjugated anti-Rabbit	Vector Laboratories	VE-MP-7401-50	
Antibody	Cy5-conjugated anti-mouse	Jackson immunoresearch	711-175-152	1 : 500

Antibody	Cy3-conjugated anti-rat	Jackson immunoresearch	712-165-153	1 : 500
Antibody	Cy5-conjugated anti-Goat	Jackson immunoresearch	705-175-147	1 : 500
Antibody	Cy2-conjugated anti-Rabbit	Jackson immunoresearch	711-255-152	1 : 200
Antibody	111Cd-CD44	Biolegend	BLG-103002	
Antibody	143Nd-CD69	FLUIDIGM	3143004B	
Antibody	145Nd-CD4	FLUIDIGM	3145002B	
Antibody	148Nd-CD103	Biolegend	BLG-121402	
Antibody	149Sm-CD19	FLUIDIGM	3149002B	
Antibody	152Sm-CD3e	FLUIDIGM	3152004B	
Antibody	153Eu-CD8a	FLUIDIGM	3153012B	
Antibody	159Tb-PD1	FLUIDIGM	3159024B	
Antibody	160Gd-CD62L	FLUIDIGM	3160008B	
Antibody	164Dy-CCR7	FLUIDIGM	3164013A	
Antibody	175Lu-IL7Ra	FLUIDIGM	3175006B	
Antibody	176Yb-ICOS	FLUIDIGM	3176014B	
Antibody	113Cd-Ki67	Biolegend	BLG-652402	
Antibody	115In-Eomes	eBioscience	14-4875-82	
Antibody	155Gd-IRF4	FLUIDIGM	3155014B	
Antibody	158Gd-Foxp3	FLUIDIGM	3158003A	
Antibody	161Dy-Tbet	FLUIDIGM	3161014B	
Antibody	167Er-Gata3	FLUIDIGM	3167007A	
Antibody	171Yb-GranzymeB	FLUIDIGM	3171002B	
Antibody	172Yb-pS6	FLUIDIGM	3172008A	
Antibody	173Yb-TCF1	R&D systems	MAB8224	
Other	FDM barcode 2,8,15,18,19,20	FLUIDIGM	201060	
Other	gentleMACS™ Dissociator	Miltenyi Biotec	130-093-235	
Other	Wash buffer	Zytomed Systems	ZUC020-50	
Other	Protein block	Abcam	ab64226	
Other	ImmPACT DAB Kit	Vector Laboratories	VE-SK-4105	
Other	Maxpar PBS	FLUIDIGM	201058	
	Maxpar Cell staining buffer	FLUIDIGM	201068	
Other	Maxpar MCP9 Antibody Labeling Kit, 111Cd	FLUIDIGM	201111A	
Other	Maxpar MCP9 Antibody Labeling Kit, 113Cd	FLUIDIGM	201113A	
Other	MIBItag Conjugation Kit_115In	IONpath	600115	
Other	MIBItag Conjugation Kit_173Yb	IONpath	600173	

Mice

All animal studies were approved by the Hebrew University Institutional Animal Care and Use Committee. Previously described ROSA26-LSL-IKKβ(EE) mice (Sasaki et al., 2006) were bred with Albumin (Alb)-Cre mice obtained from Jackson Laboratory (Bar Harbor, Maine, stock # 003574) to generate Alb-IKKβ(EE)^{Hep} mice as described previously (Finkin et al., 2015). RORc knock out mice (B6.129P2(Cg)-*Rorc*^{tm2Litt}/J) and floxed RORc mutant (B6(Cg)-*Rorc*^{tm3Litt}/J) mice were purchased from Jackson laboratories (stock # 007572 and 008771, respectively), and bred into Alb-IKKβ(EE)^{Hep} mice. The IKK RORc KO colony was kept by mating IKK RORc KO males to IKK RORc Het females. Genotyping was done according to the suppliers' protocol:

Alb-Cre: https://www.jax.org/Protocol?stockNumber=003574&protocolID=26917

IKKβ(EE): https://www.jax.org/Protocol?stockNumber=008242&protocolID=27052

Rorc^{tm2Litt}: https://www.jax.org/Protocol?stockNumber=007572&protocolID=23307

Rorc^{tm3Litt}: https://www.jax.org/Protocol?stockNumber=008771&protocolID=27794

All mice were of a pure C57BL/6J genetic background and were bred and maintained in specific pathogen-free conditions. Only male mice were used for experiments. Animals were sacrificed by a lethal dose of anesthesia and perfused through the left ventricle with heparinized PBS. For hepatocarcinogenesis, mice were injected intraperitoneally (i.p) with 10 mg/kg Diethylnitrosamine (DEN) at 14 days of age. Mice were observed for development of tumors at 6 months of age.

Human tissues

Human liver and skin biopsy specimens were obtained from the archives of the Pathology Institute, Hadassah Medical Center, Israel. The study protocol was approved by the institutional review board of Hadassah Medical Center (Ref. 0201-18-HMO) and was in accordance with the Helsinki declaration guidelines. TLSs chosen for analysis from HCC patient were located in non-neoplastic liver parenchyma [as examined by an expert liver pathologist (E.P)]. TLSs from melanoma patients were located in the vicinity of the tumors or within the tumors.

Liver immune cell isolation, staining and sorting

Immune cells were isolated from 6 months old DEN-injected mice. Immune cells were isolated from 3 IKK RORc Het mice (cells were pooled after isolation). Immune cells from 2 IKK RORc KO mice were isolated, and frozen section of one lobe from each mouse was prepared and taken immediately for H&E staining, to test for lymphoma presence within the liver. Livers were cut to small pieces in 5 ml liver digest medium, squashed with a syringe piston, and incubated at 37°c for 30 minutes. PBS was added and cells were centrifuged at 350g for 5 minutes at 4°c. Further digestion was done with Accumax+DNAse for 10 minutes at 37°c followed by neutralization with Fetal Bovine Serum (FBS) and PBS. Suspension was passed through a 70 µm mesh filter. Two centrifugations at 30g for 5 minutes at 4°c were performed to reduce the content of hepatocytes. Supernatant was then centrifuged at 350g at 4°c to precipitate the immune cells, and the pellet was resuspended in 6ml of 35% Percoll and gently placed on top of 3ml of 75% Percoll. Cells were centrifuged for 20 minutes at 900g without brake, and the ring of immune cells between the 2 Percoll concentrations was taken out into PBS and centrifuged for 8 minutes at 350g. Red blood cell lysis was performed for 2 minutes at RT and cells were resuspended in PBS+2%FBS (FACS buffer). Cells were counted using Trypan blue. Three million cells were taken for antibody staining.

Before antibody staining, blocking (FACS buffer, 1%Rat Serum, 1%Fc Blocker) was done for 10 minutes at 4°c. Cells were incubated with primary antibodies (Pacific Blue-CD45 and APC-F4/80) for 20 minutes at 4°c. Cells were washed with FACS buffer and transferred through a 35µm filter. Viability was assessed by Propidium Iodide which was added to the cells just before sorting.

$CD45^{+}F4/80^{-}PI^{-}$ cells were sorted using a BD FACSAria™ III sorter. Sorting was performed using a 85-micron nozzle and threshold was kept in the range of 3000 events/second. F4/80 positive cells (macrophage/Kupffer cells), which constitute a major part of liver immune cells, were excluded from the sort to reduce their amounts from the total CD45 positive cells and enable a better representation of lymphocytes. Cells were sorted into Eppendorf tubes containing 1ml of FACS buffer, and then centrifuged without brake. Cells were counted and brought to a concentration of 700 cells/µl.

Single cell RNA sequencing (scRNA-seq)

Cells were loaded onto a Chromium single-cell 3′ v2 chip (10x Genomics) and libraries were prepared according to the manufacturer's protocol. Libraries were sequenced by Illumina HiSeq 2500 and the reads were mapped to *mm10* library (ensembl v98). The alignment was performed using *Cellranger* (v6.1.2) (G. X. Y. Zheng et al., 2017). Downstream analysis was performed by *Seurat* (v4.0.4) R package (Hao et al., 2021). Cells with a low number of detected cDNA UMI (<1000), a low number of identified genes (<200), or a high percentage of mitochondrial genes (>10%) were filtered out. The standard single-cell processing pipeline from Seurat was used for downstream analysis. After initial clustering on the cells by UMAP, separate analyses were performed for T cells. A total of 3089 cells were analyzed for IKK RORc Het and 7698 cells for IKK RORc KO mice.

Cytometry by time of flight (CyTOF)

Immune cells were isolated from 6 months old DEN-injected mice. Immune cells from 4 IKK and from 3 IKK RORc Het mice were isolated and then pooled separately. Immune cells from 3 IKK RORc KO were isolated separately and one lobe was taken for frozen section and H&E staining immediately to test for lymphoma presence within the liver. Immune cells were isolated as described for the scRNA-seq method, except for the initial digestion steps: the liver was cut to small pieces and incubated in 5ml Liver digest medium, DNAse + Brefeldin A and samples were submitted to Gentlemax dissociation. The cells were then incubated at 37°c for 15 minutes and submitted to another step of Gentlemax dissociation.

Isolated cells were washed with CyTOF PBS and stained with Cisplatin viability stain for 2 minutes. Cells were washed twice and stained with extracellular antibodies cocktail at RT for 1 hour. After extracellular staining, cells were washed twice and fixed over night at 4°c using the Foxp3/Transcription Factor staining buffer set. All centrifugation steps after fixation were done at 700g to minimize cell loss. Cells were centrifuged, permeabilized and each sample was barcoded for 2 hours at RT. Cells were washed twice in permeabilization buffer and counted. Equal numbers of barcoded samples were united and stained with Intracellular antibodies cocktail for 1 hour RT. Cells were washed with CyTOF staining buffer and fixed in 4% PFA with Ir-193 (1:500) overnight at 4°c, followed by washes with CyTOF water. Stained

and Fixed cells were analyzed using the CyTOF 3 (Helios) system (FLUIDIGM). Data was processed using Cytobank software. A total of 133,334 cells were analyzed for each mouse.

Immunofluorescent staining

Immunofluorescence was performed on formalin-fixed paraffin-embedded (FFPE) sections. Sections were de-paraffinized in Xylene (twice for 5 minutes) and rehydrated through a series of 100%, 96% and 80% Ethanol followed by 2 washes in PBS. Antigen retrieval was done in Citrate or Tris buffers in pressure cooker (125°c, 3 minutes). Sections were rinsed twice in PBS and blocked for 2 hours at RT in blocking buffer (2% BSA, 10% Donkey serum, 0.1% Tween). Primary antibody was diluted in blocking buffer and incubated overnight at 4°c. Sections were washed in PBS 0.1% Tween, and secondary fluorescent conjugated antibody diluted in PBS 2% BSA was incubated at RT for 2 hours. Sections were washed 3 times in PBS and incubated with DAPI for 5 minutes followed by 2 washing steps. Slides were mounted in Vectashield fluorescent mounting medium. All antibodies and staining conditions can be found in the resource table.

Immunohistochemistry

Immunohistochemistry was performed on FFPE sections. Sections were de-paraffinized and rehydrated followed by 2 washes in DW. Antigen retrieval was done in Citrate or Tris buffers in pressure cooker (125°c, 3 minutes). Sections were rinsed twice in DW and incubated in 3% Hydrogen Peroxide for 10 minutes at RT followed by 3 rinses in DW. Sections were washed in wash buffer and blocked with protein block for 2 hours at RT. Sections were incubated with primary antibody diluted in protein block over night at 4°c and washed 3 times in wash buffer. Sections were incubated with HRP-conjugated secondary antibodies for 30 minutes at RT and washed in wash buffer. DAB solution was added for up to 15 minutes in the dark, and sections were rinsed in tap water. Hematoxylin staining was done for 10 to 60 seconds followed by washes in tap water. Sections were dehydrated and mounted.

Image analysis

H&E slides were scanned using the Aperio AT2 slide scanner. ImageScope software was used to quantify the abundance of TLSs and tumors and their diameters. ImageScope was also used to quantify positive cells in immunohistochemistry. Tumors were scored as HCC or iCCA

according to H&E staining. Validation of tumor type identification was done by IHC for HNF4 and CK19: HCCs were identified by HNF4 positive staining, while iCCAs were defined by lack of HNF4 expression and expression of CK19. For Immunofluorescent stainings, images were collected on a Nikon Digital Eclipse C1 confocal microscope, and analyzed using Photoshop software. Cells positive for an antibody staining (or combinations) were scored manually using "Count tool" in a field with identical area. Since the distribution of CD8 and CD4 cells in TLSs is not even, the field was placed in the most crowded area of CD8 or CD4 cells within TLSs. Between 3 and 10 TLSs were scored per mouse. Between 3 and 6 TLSs were scored per patient. In all graphs showing quantification of immunostaining, each data point represents an average of several TLSs in a single mouse. In all graphs showing quantification of TLSs and tumors, all the TLSs and tumors in two sections representing the entire liver were counted, and each data point represents a single mouse.

Statistical analysis

Statistical analysis was performed by an expert statistician (Tali Bdolah-Abram). The comparison of a quantitative variable between two independent groups was performed by using the non-parametric Mann-Whitney test. The comparison of a quantitative variable between three or more independent groups was carried out by using the non-parametric Kruskal-Wallis test. The Bonferroni correction of the significance level was applied to Post-Hoc tests. Non-parametric tests were used due to the small sample sizes used in the experiments.

All statistical tests were two-tailed, and a p-value of 5% or less was considered statistically significant. Levels of significance are indicated as $*p < 0.05$; $**p < 0.01$; $***p < 0.001$. Statistical details for all experiments can be found in the respective figure legends. All graphs show Box plots representing Median, Maximum and Minimum values. Graphs were generated using the Seurat package for R, Cytobank, Excel and GraphPad Prism 6.0 software. Significance is not indicated for scRNA-seq and CyTOF experiments due to small sample sizes, yet similar results obtained using both methods, and validation of some of the results by immunostainings, strengthen their validity.

Results:

RORc expressing cells are not necessary for TLS neogenesis but rather negatively regulate their formation

IKKβ(EE)^{Hep} mice drive a constitutively active form of IKKβ in hepatocytes which mimics chronic inflammation (Finkin et al., 2015). Few dispersed RORc positive cells were detected within TLSs forming in the liver of IKKβ(EE)^{Hep} mice (Fig. 1A, arrowhead, inset). In order to test whether RORc expressing cells are necessary for hepatic TLS neogenesis in IKKβ(EE)^{Hep} mice, we crossed IKKβ(EE)^{Hep} mice (denoted here IKK) with whole body RORc knock out mice (RORc^{tm2Litt} KO mice, denoted here RORc KO) (Eberl et al., 2004). These mice will be referred to as IKK RORc KO mice. The controls used were: RORc heterozygous (RORc Het) or homozygous mice (RORc KO), as well as IKK RORc Het mice (IKK RORc Het behaved similarly to IKK mice). RORc KO mice develop T cell lymphomas (Ueda et al., 2002), thus to avoid lymphoma affecting the analysis of liver TLSs, mice which at the date of sacrifice showed an enlarged thymus and spleen, or histological evidence of hepatic lymphoma, were omitted from the analysis. The remaining mice, which did not develop T cell lymphomas, were analyzed for hepatic TLS and tumor abundance in several conditions: A) at 6 and 12 months of age without carcinogen treatment (termed 'spontaneous'). As reported previously, under these conditions IKK mice develop TLS-containing tumor progenitors that grow in number and size as a function of time, with tumors appearing after 1 year of age. B) At 6 months of age following a single injection of the carcinogen Diethylnitrosamine (DEN) at 14 days of age, to accelerate TLS and tumor formation, and therefore DEN-injected IKK mice develop at this age both TLSs and tumors (Finkin et al., 2015)(Tolba et al., 2015).

Spontaneous and DEN-injected IKK RORc KO mice did not lose the ability to develop liver TLSs harboring tumor progenitors, typical to IKK RORc Het mice, indicating that RORc expressing cells are not necessary for TLS development in this setting. On the contrary, the abundance of TLSs with tumor progenitors was significantly increased in IKK RORc KO mice compared to IKK RORc Het mice [median=17.85 compared to 0.65 (6mon – DEN), median=21.32 compared to 3.91 (6mon + DEN) and median=23.34 compared to 1.69 (12mon – DEN), respectively] (Fig. 1B and C, Fig. S1A and S2). Tumor progenitors within TLSs are clearly apparent in the H&E staining of both IKK RORc Het and IKK RORc KO mice and were also identified by the

expression of the tumor progenitor markers Sox9 and CD44v6 in epithelial cells expressing E-cadherin (Fig. 1D). As expected, TLSs in IKK RORc KO mice lack RORc positive cells (Fig. 1A). These results suggest that RORc expressing cells are not necessary for TLS neogenesis in IKK mice; rather, RORc expressing cells negatively regulate TLS formation.

In IKK mice TLSs increased in size with time in both spontaneous and DEN-injected mice (Finkin et al., 2015). Similarly, in IKK RORc KO mice, DEN treatment or prolonged time (12mon) facilitated the formation of larger sized-TLSs (200-400μm in diameter). However, spontaneous IKK RORc KO mice at 6 months develop only small sized TLSs (0-200μm in diameter) but not larger ones (200-400μm in diameter) (Fig. S1C). This suggests that RORc expressing cells control TLS neogenesis rather than TLS growth.

Interestingly, in IKK RORc Het mice DEN administration or older age (12 months) promoted formation of TLS harboring tumor progenitors compared to spontaneous 6 months old mice. However, in IKK RORc KO mice, neither DEN administration nor aging contributed to a further increase in TLS number (Fig. 1B). The carcinogen-independent development of TLSs harboring tumor progenitors suggests an existence of a strong driving force for TLS neogenesis in the absence of RORc expressing cells.

Spontaneous and DEN-injected RORc KO mice showed accumulation of small TLS-like structures in the liver (less than 200μm in diameter) (Wichner et al., 2013) (Fig. 1C,D and Fig. S1B), mainly adjacent to central veins. Notably, TLSs forming in RORc KO mice did not harbor tumor progenitors (Fig. 1D and Fig. S1A,B). The number of TLSs (lacking liver tumor progenitors) in RORc KO mice increased with time and following DEN treatment (Fig. S1B). IKK RORc KO mice, in all conditions, harbored high numbers of both TLSs lacking tumor progenitors and TLSs harboring tumor progenitors, the latter being around 2 to 4 fold more abundant than the former.

Thus, RORc expressing cells are not necessary for TLS neogenesis but rather negatively regulate the neogenesis of TLSs in the liver.

Intrahepatic cholangiocarcinoma (iCCA) load is decreased in IKK mice lacking RORc expressing cells

We have previously shown that HCCs form in both IKK and wild type (WT) mice treated with DEN (Finkin et al., 2015). However, IKK, but not WT mice, develop aggressive iCCAs which appear under both spontaneous and DEN treated conditions. This suggests that iCCAs are TLS-driven. Indeed, TLSs formed in IKK mice are pro-tumorigenic since in the absence of lymphocytes (in a Rag1$^{-/-}$ background), TLSs are not formed and there is a significant decrease in iCCA numbers (Finkin et al., 2015). We expected that in 6 months old DEN-treated IKK RORc KO mice, where the numbers of TLSs are significantly increased, tumor number will increase accordingly. Surprisingly, despite a 5.5-fold increase in TLS numbers, tumor formation decreased compared to IKK RORc Het mice. While HCC formation was not affected (Fig. 2A,A',C,D,D',F,G), iCCA formation was significantly decreased (Fig. 2A,A',B,D,D',E,H) (the median number of iCCAs per cm^2 formed in IKK RORc Het mice was 1.07 compared to only 0.22 in IKK RORc KO mice, p=0.03). Thus, while TLSs formed in IKK RORc Het mice are associated with an increased number of iCCAs, supernumerary TLSs in IKK RORc KO mice are less supportive for formation of iCCA. These results suggest that the phenotype of the TLSs has changed from pro-tumorigenic in IKK RORc Het mice, to anti-tumorigenic in IKK RORc KO mice. Thus, we hypothesized that RORc expressing cells might directly or indirectly control the phenotype of hepatic TLSs.

Both RORγ and its shorter isoform, RORγt, are deleted in RORc KO mice. While RORγt is expressed specifically in the immune compartment, RORγ is expressed in many cell types including hepatocytes (Eberl, 2017). RORγ expression is enhanced in HCC patients with HBV infection and overexpression of RORγ in liver cancer cells can enhance their migration and proliferation *in vitro* (Y. Huang et al., 2019). Thus, we wanted to rule out a possible contribution of knocking out RORc expression in hepatocytes to the phenotype of IKK RORc KO mice. We therefore used a floxed RORc mutant (RORc^{tm3Litt}) to eliminate RORc specifically in hepatocytes using Albumin-Cre, which is also used to drive the IKK transgene (resulting in IKK RORc$^{HepKO/HepKO}$ mice). IKK RORc$^{HepKO/HepKO}$ mice do not show a difference in either TLS, HCC or iCCA abundance compared to IKK RORc$^{wt/HepKO}$ controls (Fig. 2I), suggesting that hepatic expression of RORc is not responsible for controlling TLS or liver cancer development in IKK

mice. Thus, the increase in TLS neogenesis and the decrease in iCCA formation observed in IKK RORc KO mice is likely due to the elimination of RORc in the immune compartment.

Taken together this suggests that RORc expressing immune cells facilitate the pro-tumorigenic functions of hepatic TLSs. This could explain observations that suggest that hepatic TLSs in human tissues may be either pro- or anti-tumorigenic.

Transcriptional analysis reveals enrichment of CD8 cells with an exhausted/effector phenotype in livers of IKK RORc KO mice

Our findings provided us with a unique model system enabling us to compare "bad" pro-tumorigenic TLSs and "good" anti-tumorigenic TLSs in a similar setting. To this end, we performed single cell RNA sequencing (scRNA-seq) of isolated CD45 positive cells from livers of 6 months old DEN-injected IKK RORc Het (n= pool of 3 mice) and IKK RORc KO (n=2) mice, since we are unable to isolate immune cells specifically from TLSs. Total liver immune cells reflect at least in part the immune composition of TLSs. Hepatic immune cell populations from both genotypes included B cells, Plasma cells, CD4 and CD8 T cells, NK cells, monocytes/macrophages and granulocytes (Fig. 3A). However, we found a significant enrichment of CD8 T cells in IKK RORc KO mice compared to IKK RORc Het mice (Fig. 3A-F). In order to better identify the subpopulation of T cells, we performed a separate analysis only on T cells; this analysis demonstrated a clear distinction between T cell populations from IKK RORc Het versus IKK RORc KO mice (Fig. 3B,C). T cell analysis was able to differentiate between different CD8 expressing cell clusters, of which cluster 0 was the most enriched (15.1-fold) in IKK RORc KO mice and represents CD8 effector cells with both exhaustion and effector markers ($CD8_{EX/EFF}$) (Fig 3B-F). Other enriched CD8 cell clusters included CD8 resident memory ($CD8_{RM}$) cells (cluster 6, enriched 4.4-fold), CD8 memory ($CD8_{MEM}$) cells (cluster 1, enriched 1.7-fold), and a small cluster of proliferating CD8 cells (cluster 9, enriched 4-fold) (Fig. 3B-F). Other CD8 clusters, including naïve (cluster 2) and central memory ($CD8_{CM}$) (cluster 4), were reduced in IKK RORc KO compared to IKK RORc Het mice, while two clusters of activated effector CD8 cells (cluster 7) and CD8 cells with a signature of type1 interferon (IFN) response (cluster 11) were unchanged (Fig. 3B-F).

The reduction in CD8 naïve cells and enrichment of the effector/memory CD8 cells suggests there is an active process of antigen recognition and differentiation of CD8 cells from the

naïve pool, that is more pronounced in IKK RORc KO mice compared to IKK RORc Het mice. CD8 cells in the tumor microenvironment have been shown to undergo a process of exhaustion whereby they upregulate the expression of multiple inhibitory receptors, and gradually loose effector functions (Pauken & Wherry, 2015). Since immune cells in TLSs are in close proximity to tumor progenitors, we asked whether the enriched CD8 cells have elevated expression of exhaustion markers. Cluster 0 of effector CD8 cells ($CD44^+$ $CD62L^-$ $CCR7^-$ $IL7r^-$), which is most strongly enriched in IKK RORc KO mice, expressed some exhaustion markers such as PD-1, Lag3, Tox and Ikzf2 (Fig. 3G and Fig. S3). However, this cluster also highly expressed cytotoxic markers such as Perforin, Granzyme A, B and K (Gzma, Gzmb, Gzmk), as well as IFNg (Fig. 3G and Fig. S3), suggesting it is not terminally exhausted but rather retains effector functions. Similarly, the enriched cluster 6, which was identified as $CD8_{RM}$ cells by the expression of CD103 and CD69, expressed the anti-tumor cytokines IFNg and TNF (Fig. 3C, E-G and Fig. S3).

CD4 Naïve cells (cluster 3) are less abundant in IKK RORc KO mice compared to controls, similarly to CD8 Naïve cells. Two other CD4 clusters were identified: a pro-inflammatory cluster 5 which is $IL\text{-}7r^+$ $IL\text{-}2^+$ and an anti-inflammatory cluster 8 which is $IL\text{-}7r^-$ $IL\text{-}10^+$ (Fig. S3). However, both clusters expressed markers of T follicular helper (T_{FH}) cells such as Maf, Ox40, CD40L and ICOS (Fig. S3), suggesting that T_{FH} cells along with other CD4 cell types compose these clusters. While IL-2 expressing CD4 cells were distributed evenly in IKK RORc Het and IKK RORc KO mice, IL-10 expressing CD4 cells tended to be enriched (5-fold) in IKK RORc KO mice. IL-10 producing $IL\text{-}7r^-$ induced regulatory T cells have been identified in human blood (Häringer et al., 2009) and similar $Foxp3^-$ regulatory (Tr1) T cells were shown to modulate the inflammatory response to malaria (Couper et al., 2008). Thus, cluster 8 might represent such suppressive Tr1 cells that rise in IKK RORc KO mice. Tregs expressing Foxp3 clustered separately (cluster 10) but were not significantly changed between IKK RORc KO and controls (Fig. 3B-F and Fig. S3). Interestingly, very few $RORc^+$ cells were identified in a distinct part of the $CD4^+$ Cluster 5 (Fig. S3) that seems to be $CD3^+CD4^-CD8^-$, which suggests that most $RORc^+$ expressing cells in IKK RORc Het mice possibly represent $\gamma\delta$T cells [and not ILC3 ($CD3^-$) or Th17 ($CD3^+$ $CD4^+$ cells)]. As expected, this part of cluster 5 was not detected in IKK RORc KO mice.

Altogether, the increase in CD8 cell populations with cytotoxic potential and CD4 cells with regulatory functions suggest an ongoing process of antigen recognition. This process could

target potential cancer antigens in IKK RORc KO mice and may explain the anti-tumorigenic phenotype of TLSs in this background.

RORc expressing cells control the abundance and phenotype of CD8 effector and memory T cells

To further delineate T cell states at the protein level we employed Cytometry by time of flight (CyTOF) with 21 T cell markers. Similarly to the scRNA-seq results, CyTOF analysis of immune cells isolated from whole livers of 6 months old DEN-injected IKK RORc Het and IKK RORc KO mice showed an enrichment of CD8 cells in IKK RORc KO mice compared to IKK RORc Het mice. CD8 effector ($CD8_{EFF}$), $CD8_{MEM}$ and $CD8_{RM}$ populations were increased in IKK RORc KO compared to controls, as observed in the scRNA-seq analysis (Fig. 4A,B and Fig. S4). In the CD4 populations, $CD4_{MEM}$, Treg ($Foxp3^+$) and T_{H2} ($Gata3^+$) cell populations decreased in IKK RORc KO while T_{H1} ($Tbet^+$), T_{FH} ($ICOS^+$) and T_{RM} ($CD103^+CD69^+$) increased compared to IKK RORc Het mice (Fig. 4C,D and Fig. S4). As seen in the scRNA-seq analysis, a population of $CD3^+$ $CD8^-CD4^-$ [CD3 Double Negative ($CD3_{DN}$)] cells decreased in IKK RORc KO compared to IKK RORc Het mice, suggesting this population might partially be comprised of $\gamma\delta$T $RORc^+$ expressing cells (Fig. 4A,E). IKK RORc KO mice show a slight decrease in B cell frequencies although not pronounced. A population of $CD19^{-/+}$ $IRF4^+$ $Ki67^+$ cluster which probably represents plasmablasts (Tellier & Nutt, 2017) was enriched in IKK RORc KO (Fig. 4F,G and Fig. S4), again supporting ongoing antigen recognition in 'good' TLSs in IKK RORc KO mice.

Two populations of exhausted T cells have been previously identified in the tumor microenvironment: a progenitor population ($PD1^+Tbet^+Eomes^-$) with greater polyfunctionality and the ability to persist in the absence of antigen, as well as a terminally exhausted population ($PD1^+Tbet^-Eomes^+$) with superior cytotoxicity but reduced long-term survival. The progenitor population gives rise to terminally exhausted T cells, mediates enhanced tumor control and retains responsiveness to PD-1 blockade (Miller et al., 2019)(Paley et al., 2012; Pauken & Wherry, 2015). A recent study by Kim et al. has shown that tumors with high-$PD1^{high}$ signature, which correlated with $PD1^{high}$ tumor- infiltrating CD8 T cells, were associated with poorer survival outcomes in HCC patients. They further show that $PD1^{high}$ tumor-infiltrating CD8 T cells have marked enrichment of exhaustion-related genes compared with $PD1^{intermediate}$ and $PD1^{negative}$ tumor-infiltrating CD8 T cells. The $PD1^{high}$ subpopulation had the lowest

proportion of Tbet^{high}/Eomes^{low} cells (Kim et al., 2018). We thus divided the CD8$_{EFF}$ and CD8$_{MEM}$ populations to PD1^{high}, PD1^{int} and PD1^{-} expressing cells. We found that in both IKK RORc KO and controls the majority of the cells in both CD8$_{EFF}$ (median=63.6% in IKK RORc Het and 70.2% in IKK RORc KO) and CD8$_{MEM}$ (median=72.6% in IKK RORc Het and 83.3% in IKK RORc KO) was PD1 negative, suggesting they are not exhausted. The percent of cells expressing PD1^{high}, PD1^{int} and PD1^{-} in CD8$_{EFF}$ cells, is similar between controls and IKK RORc KO mice (Fig. 5A,B). However, in CD8$_{MEM}$ cells the percent of cells expressing PD-1^{int} is lower in IKK RORc KO compared to controls (median=20.49% in IKK RORc Het and 11.13% in IKK RORc KO) (Fig. 5B), suggesting CD8$_{MEM}$ are less exhausted in IKK RORc KO. We find that the proportion of Tbet^{+} Eomes^{-} cells decreases as PD1 levels increase at least in IKK RORc KO, as described previously (Fig 5D). However, the proportion of Tbet^{+} Eomes^{-} PD1^{int} and Tbet^{+} Eomes^{-} PD1^{-} cells was higher in IKK RORc KO compared to IKK RORc Het mice in both CD8$_{EFF}$ and CD8$_{MEM}$ cells (Fig. 5A,D,F,H), suggesting that CD8$_{EFF}$ and CD8$_{MEM}$ are less exhausted in IKK RORc KO compared to IKK RORc Het mice.

In the tumor microenvironment, TCF1 (encoded by *Tcf7*) expression in both CD8^{+}PD1^{-} (Sade-Feldman et al., 2018)(Kurtulus et al., 2019) and CD8^{+}PD1^{+} cells (Siddiqui et al., 2019), has been reported as a marker of a progeny subset that is better in tumor growth control than terminally exhausted TCF1-negative CD8 cells. In IKK RORc Het, as well as in IKK RORc KO mice, the majority of the PD1^{high}, PD1^{int} and PD1^{-} cells in CD8$_{EFF}$ and CD8$_{MEM}$ express TCF1 although there was no difference in their abundance between IKK RORc Het and IKK RORc KO mice (Fig. 5A,E,G). This supports the possibility that these cells are not terminally exhausted and might be able to control tumor growth.

The mTOR pathway is pivotal for complete T cell activation and induces potent effector functions (Y. Zheng et al., 2007). We find that the percentage of CD3$_{EFF}$ PD1^{high} and CD8$_{MEM}$ PD1^{high} cells expressing pS6, the downstream effector of the mTOR pathway, is higher in IKK RORc KO compared to IKK RORc Het mice (Fig. 5A,D,F,H). Moreover, the percentage of CD3$_{EFF}$ PD1^{high} and CD8$_{MEM}$ PD1^{high} cells expressing the cytotoxic marker Granzyme B (GzmB) are similarly higher in IKK RORc KO compared to IKK RORc Het mice (Fig. 5A,D,F,H). These results suggest that exhausted PD1^{high} CD8 cells possess effector functions and their abundance is higher in IKK RORc KO mice compared to controls, potentially enabling more efficient tumor cell killing.

Recently, a novel role was found for the zinc-finger transcription factor Gata3 as a driver of $CD8^+$ T cell dysfunction (Singer et al., 2016). We find that the percentage of Gata3 expressing $CD8_{MEM}$ cells is lower in IKK RORc KO mice compared to IKK RORc Het mice (Fig. 5C,H and Fig. S4). These results are in line with our previous findings and suggest that CD8 cells in IKK RORc KO are less dysfunctional compared to controls.

Altogether, our results suggest that in IKK RORc KO mice, CD8 cells with an exhausted yet cytotoxic potential are enriched compared to IKK RORc Het mice. Moreover, there is a shift from pro-tumorigenic to anti-tumorigenic CD4 cell types in IKK RORc KO compared to controls. These changes in the immune phenotypes of hepatic lymphocyte populations might favor an anti-tumorigenic milieu in IKK RORc KO mice. Thus, $RORc^+$ cells negatively regulate CD8 cells abundance and favor a more exhausted and less cytotoxic CD8 phenotype, most likely promoting tumor growth.

Anti-tumorigenic TLSs are enriched in exhausted, yet proliferative, CD8 cells with a progenitor phenotype

Both our scRNA-seq and CyTOF results revealed an enrichment of CD8 cells in livers of IKK RORc KO compared to IKK RORc Het mice. In order to test if CD8 enrichment is indeed occurring within the TLSs, we stained for CD8 by immunohistochemistry. In IKK RORc Het mice CD8 cells are dispersed across small TLSs (< 350μm in diameter), however they partly crowd together in big TLSs (> 350μm in diameter), not enabling accurate quantification. We therefore focused our analysis on small TLSs. We find that CD8 cell abundance increases (3-fold) in small TLSs of IKK RORc KO mice compared to IKK RORc Het mice (Fig. 6A,B). In order to test the exhaustion state of these CD8 cells, we co-stained liver sections for CD8, PD1 and the proliferation marker Ki67, a combination that marks cellular proliferation and T cell reinvigoration upon checkpoint blockade treatment (A. C. Huang et al., 2017). Proliferating $CD8^+$ $PD1^+$ cells have been identified recently as part of a T_{EX}^{prog2} population which differentiates into T_{EX}^{int} cells that has similarities to circulating “effector-like” cells. These cell types were distinct from a terminally exhausted cell type, T_{EX}^{term} (Beltra et al., 2020). We found a significant increase in $CD8^+$ $PD1^+$ (6.5-fold), $CD8^+$ $Ki67^+$ (4.8-fold) and $CD8^+$ $PD1^+$ $Ki67^+$ (5-fold) cells in TLSs of IKK RORc KO compared to IKK RORc Het mice (Fig. 6A,B). When normalized to CD8 numbers, 13.7% of CD8 cells are positive for PD1 in TLSs of IKK RORc Het

mice while in IKK RORc KO they rise to 24.5%. $CD8^+$ $PD1^+$ $Ki67^+$ make up 3.3% of CD8 cells within TLSs of IKK RORc Het mice, and they rise to 6.2% of CD8 cells in TLSs of IKK RORc KO mice, however this difference is not significant. Thus, the increase in numbers of $CD8^+$ $PD1^+$ $Ki67^+$ cells is in line with the general increase in total CD8 cells. Therefore, TLSs in IKK RORc KO mice harbor more CD8 cells which are exhausted, yet proliferative, compared to IKK RORc Het mice. The abundance of CD4 cells in TLSs was also analyzed together with PD1 and Ki67 expression, showing a non-significant 2-fold increase in CD4 cells in TLSs of IKK RORc KO compared to controls (Fig. S5A,C). A 2.7 fold increase in $CD4^+$ $PD1^+$ $Ki67^+$ cells is seen in TLSs although it is not significant (Fig. S5A,C).

Moreover, as identified in the CyTOF analysis, most of the CD8 cells express the progenitor marker TCF1 (52.7% in IKK RORc Het and 70% in IKK RORc KO). The percentage of cells expressing $CD8^+$ $TCF1^+$, and $CD8^+$ $TCF1^+$ $PD1^+$ increases 4-fold and 5-fold, respectively, in IKK RORc KO compared to controls (Fig.6A,C). This increase reflects the total increase in CD8 cells since it is not significant when normalized to CD8 cell numbers. This suggests that within TLSs, the abundance of CD8 cells that are not terminally exhausted and have a more progenitor phenotype is higher in IKK RORc KO.

T cell activity in TLSs has been shown to be inhibited by Tregs in the context of lung adenocarcinoma (Joshi et al., 2015). PD1 expression on Tregs is important for Treg cell homeostasis and function (Kumar et al., 2019). We thus determined if Treg cell abundance and expression of PD1 could be at the basis of the difference between TLSs in IKK RORc Het and IKK RORc KO mice. However, we observe no difference in the numbers of either $Foxp3^+$ or $Foxp3^+$ $PD1^+$ cells in TLSs of controls compared to IKK RORc KO mice (Fig. S5B,C). This suggests that Treg abundance is probably not the reason for the differences in the phenotype of TLSs observed in IKK RORc KO versus controls. In our CyTOF analysis (but not in the scRNA-seq) we observed a decrease in Tregs in IKK RORc KO compared to controls. This could reflect changes in Treg abundance in non-TLS regions of the liver. Similarly, another population of suppressive cells, the myeloid-derived suppressor cells (MDSCs), are very scarce and show no difference in numbers in TLSs of IKK RORc KO compared to controls (Fig. S5D).

Exhausted CD8 cells are more proliferative in TLSs of melanoma patients compared to HCC patients

Our results suggest that one of the differences between pro-tumorigenic and anti-tumorigenic TLSs might stem from the abundance of CD8 cells with a less exhausted and more proliferative progenitor like phenotype within TLSs. In order to test if this phenomenon is also relevant to human TLSs, we compared TLSs that develop in melanoma patients, which were reported as anti-tumorigenic (Messina et al., 2012), to peri-tumoral TLSs in HCC patients which were reported as pro-tumorigenic (Finkin et al., 2015). We find that TLSs in melanoma patients have a higher abundance of $CD8^+$ (2.5-fold), $PD1^+$ (1.7-fold) and $Ki67^+$ (4.7-fold) cells (Fig. 7A,B). Moreover, the abundance of double positive $CD8^+$ $Ki67^+$ cells is 16.3-fold higher and that of triple positive $CD8^+$ $PD1^+$ $Ki67^+$ cells is 22-fold higher in melanoma compared to HCC patients (Fig. 7A,B). When normalized to CD8 numbers, $CD8^+$ $Ki67^+$ cells increase 6.5-fold and $CD8^+$ $PD1^+$ $Ki67^+$ cells increase 9-fold in melanoma versus HCC. Thus, the numbers and functional capacity of TLS residing CD8 T cells is associated with TLS function in human tumors, similar to our findings in the mouse model.

Discussion:

TLSs have prognostic and predictive value in cancer: they mostly predict a favorable outcome, but also in few cases, including liver cancer, are associated with a poor prognosis (Sautès-Fridman et al., 2019). Recent studies provided evidence for a predictive value of TLSs in response to immune check point blockers (ICB). TLSs either directly contribute to the ICB response or report on a tumor microenvironment that is permissive to ICB (Schumacher & Thommen, 2022). Thus, manipulation of TLS neogenesis could have great therapeutic implications. In this study, we report for the first time a genetic manipulation that greatly enhanced TLS neogenesis in the context of liver cancer. We find that mice with chronic liver inflammation, that are devoid of RORc, develop supernumerary TLSs. Although excess TLSs harboring tumor progenitors develop in this background, these TLSs do not promote tumorigenesis, but on the contrary, are anti-tumorigenic. Thus, this genetic manipulation not only increased the number of TLSs, but also changed their phenotype from pro- to anti-tumorigenic. Using a combination of transcriptomic, proteomic and immunohistochemical analyses, we find that RORc expressing cells inhibit the accumulation CD8 cells with partially exhausted phenotype that maintain expression of cytotoxic effectors and have a more

progenitor-like proliferative phenotype. Moreover, RORc expressing cells promote a T_{H2} over T_{H1} phenotype of CD4 cells. This immune regulation might account for the anti-tumorigenic nature of TLSs forming in the absence of RORc. Importantly, a comparison between human pro- and anti-tumorigenic TLSs revealed an increase in CD8 abundance and in proliferating $PD1^+$ expressing CD8 cells in anti-tumorigenic TLSs, as seen in mice. This suggests that maybe CD8 abundance within TLSs and their exhausted/proliferative state could act as biomarkers to differentiate between pro- and anti-tumorigenic TLSs. In the future, manipulating RORc expressing cells or subsets of CD8/CD4 cells might offer an avenue of regulation of TLS abundance and phenotype.

Which cell type functions as LTi like cells in the absence of RORc?

We find that $RORc^+$ expressing cells are not necessary for TLS neogenesis in IKK RORc KO mice. Surprisingly, we even find that they negatively regulate the numbers of TLSs formed. One report has previously described excess TLS formation in the colon of RORc KO mice which was aggravated upon dextran sulfate sodium (DSS)-induced intestinal inflammation. Antibiotic treatment reduced supernumerary TLS formation suggesting that the increased TLS formation served as a compensatory mechanism in order to restrain the intestinal microbiota (Lochner et al., 2011). In our model, one could hypothesize that $RORc^+$ cells normally inhibit the activity or abundance of another cell population that is required for liver TLS neogenesis. Upon RORc deletion this population will increase in number and induce the formation of supernumerary TLSs. Our results show that several cell types (T_{FH}, T_{H1}, $CD4_{RM}$, $CD8_{EFF}$, $CD8_{MEM}$ and $CD8_{RM}$) are increased upon RORc deletion, and these cell types could be involved in TLS neogenesis and act as LTi cells. Recently, both T_{FH} and $CD8_{RM}$ expressing CXCL13 have been shown to promote TLS formation in human tumors (Chaurio et al., 2022)(Workel et al., 2019). Specific depletion of cell subsets in an IKK RORc KO background would be needed in order to answer this open question.

RORc expressing cells may regulate iCCA formation indirectly by regulating CD8 and CD4 cells

$RORc^+$ cells are present within TLSs and are therefore in close proximity to tumor progenitor cells. However, although we have not ruled it out, we do not favor the possibility that $RORc^+$ cells directly promote tumor progenitor growth. We observe many changes in the immune

profile of liver immune cells in IKK mice lacking RORc, that support the possibility of an indirect effect. Wichner et al. have reported spontaneous immune activation in RORc KO mice, as demonstrated by partially elevated systemic cytokine levels and enhanced frequencies of peripheral effector memory CD4 and CD8 cells and IFNg-producing CD4 cells (Wichner et al., 2013). In line with immune activation seen in RORc KO mice, we observe an increase in liver exhausted/cytotoxic CD8 cells, increase in IFNg-expressing $CD8_{RM}$ and shift from T_{H2} to T_{H1} in CD4 cells in anti-tumorigenic TLSs of IKK RORc KO mice, which could explain a greater potential of these cell compositions to kill tumor progenitors.

Our CyTOF results showed that $CD8_{EFF}$ and $CD8_{MEM}$ cells in IKK RORc KO mice have higher percentages of $Tbet^{+}Eomes^{-}$ cells, especially in the $PD1^{-}$ and $PD1^{int}$ population. Tbet is associated with good prognosis in HCC (Chew et al., 2012) and there is an inverse relationship between Tbet and PD1 expression in HCC, suggesting that Tbet modulates PD1 expression (Chew et al., 2017). Moreover, our results show that although enriched CD8 cells in IKK RORc KO mice express exhaustion markers, they also express several cytotoxic markers including Granzyme B. In line with the enrichment of CD8 cells seen in our CyTOF and scRNA-seq data, we find an increase in CD8 cells within small TLSs, which probably represent newly formed TLSs compared to bigger ones. In these small TLSs we see a more progenitor like, proliferating population that is enriched in IKK RORc KO, suggesting newly formed TLSs are more potent in controlling tumor progenitor growth in the absence of RORc.

Both our scRNA-seq and CyTOF results show an enrichment of CD8 resident memory cells in IKK RORc KO mice. CD8 resident memory cells expressed IFNg and TNF, at least at the RNA level, suggesting they can express inflammatory cytokines and may be anti-tumorigenic. Chew et al. reported that CD8 resident memory cells are critical in controlling HCC progression: They find $PD\text{-}1^{+}$ $CD8_{RM}$ cells were the predominant T-cell subset responsive to anti–PD1 treatment and were significantly reduced in number with increasing HCC tumor progression (Chew et al., 2017).

We observed that not only the CD8 population was changed in the absence of RORc, but also the CD4 population. Our CyTOF results show a shift from a T_{H2} to T_{H1} phenotype in IKK RORc KO compared to IKK RORc Het mice, although this needs further validation. Perturbation of RORc was shown to contribute to the activation of signature genes from other CD4 T cell lineages, mainly of T_{H1} ($Tbet^{+}$) cells (Xiao et al., 2014). Indeed pro-inflammatory T_{H1} cells are

usually anti-tumorigenic and T_{H2} anti-inflammatory cells are pro-tumorigenic (Hamilton & Bretscher, 2008), suggesting that this higher T_{H1}/T_{H2} ratio is overall anti-tumorigenic and might help to reduce iCCA development.

The increase in T_{FH} cells in IKK RORc KO mice suggests these cells might drive the differentiation of B cells into antibody-secreting cells (Hutloff, 2018). In accordance with this observation, we see an increase in IRF4$^+$ expressing plasmablasts in IKK RORc KO compared to IKK RORc Het mice. Indeed, several recent studies pointed to the role of TLS residing B cells in cancer immunology in general and in the response to ICBs in particular (Griss et al., 2019)(Cabrita et al., 2020)(Helmink et al., 2020)(Petitprez et al., 2020). A more detailed B cell oriented analysis will be needed to establish if a B cell dependent response is involved in the development of anti-tumorigenic TLSs.

Thus, RORc expressing cells might regulate CD8 and CD4 cell abundance and phenotype in TLSs which might, in turn, favor an anti-tumorigenic milieu. In accordance with an indirect role for RORc$^+$ cells in regulating tumorigenesis, NCR$^-$ILC3 have been previously shown to promote HCC by promoting CD8 T cell apoptosis and limiting their proliferation (Liu et al., 2019).

RORc expressing cells promote iCCA development

DEN treated IKK mice develop both DEN-derived HCC tumors (that are independent of the IKK transgene) and IKK dependent TLS-derived tumors which are mostly iCCAs and possibly also HCCs (Finkin et al., 2015). The specific effect of RORc KO on iCCA tumors and not on HCC tumors suggests that RORc$^+$ cells exert their pro-tumorigenic role only on TLS-derived iCCAs. RORc$^+$ cells suppress the accumulation of CD8 cells in TLSs and thus probably enable the growth of iCCAs. What is known about the contribution of RORc$^+$ cells to liver cancer development? RORc KO mice fail to develop several cell types including LTi, Th17, ILC3 and $\gamma\delta$T cells. Although IL-17$^+$ producing cells have an ambiguous role in cancer development, in the context of HCC the presence of Th17 cells has been correlated with poor survival (Kuen et al., 2020). $\gamma\delta$T cells producing IL-17a were shown to promote DEN induced HCC by promoting the suppressive activity of MDSCs to reinforce suppression of CD8 antitumor response (Ma et al., 2014). NCR$^-$ILC3 cells promoted the development of DEN induced HCC in response to interleukin 23 (IL-23) by producing IL-17 and directly inhibiting CD8 T cell immunity (Liu et al.,

2019). Thus, both NCR$^-$ILC3 and γδT RORc expressing cells can either directly or indirectly affect CD8 activity and regulate HCC formation. Although these cell types were shown to regulate DEN induced HCC formation, we did not observe a decrease in HCC formation in DEN injected RORc KO mice compared to RORc Het mice (both lacking the IKK transgene), as was expected if RORc$^+$ IL-17$^+$ cells promoted HCC development. Moreover, there was no difference in HCC abundance in IKK RORc KO mice compared to IKK RORc Het mice suggesting that even under chronic inflammation RORc$^+$ cells do not contribute to HCC promotion. The difference in results might stem from the fact that the other studies have used IL-17 KO mice and not RORc KO mice. While we do not observe an effect of RORc$^+$ cells on HCC development, it could still be that γδT or NCR$^-$ILC3 RORc$^+$ cells within TLSs regulate CD8 cell phenotype, and as a consequence, iCCA formation. The identity of the RORc$^+$ expressing cells that regulate iCCA formation in this model still remains to be determined, although our data suggest they could be γδT cells, since in the scRNA-seq analysis, RORc$^+$ cells were CD3$^+$CD8$^-$CD4$^-$ and in the CyTOF analysis this population decreased significantly in IKK RORc KO compared to controls.

The role of TLSs in iCCA development is largely unknown, however, a recent paper reported that high intra-tumoral abundance of TLSs is correlated with favorable prognosis, while a high abundance of peri-tumoral TLSs is correlated with a bad prognosis in patients with iCCA. Moreover, they found that T_{FH} and Treg cells were more abundant in intra-tumoral TLSs (Ding et al., 2022). Their findings in human tissues regarding T_{FH} cells are in line with our mouse data and support the notion that TLSs can be either pro- or anti-tumorigenic. The higher numbers of Treg cells in the 'favorable' intra-tumoral TLSs is however not in line with our mouse data, where we did not observe differences in Treg cell abundance in TLSs. In our mouse model we observe mainly peri-tumoral TLSs, but we find that although their location is not altered, their phenotype and cellular composition changes upon RORc deletion. The appearance of TLSs harboring tumor progenitors prior to tumor formation in IKK mice suggests that these peri-tumoral TLSs promote iCCA formation. In spite of their peri-tumoral location, these TLSs can transform into anti-tumorigenic TLSs in the absence of RORc. This suggests that TLSs do not necessarily need to be located within tumors in order to act in an anti-tumorigenic manner. Many RORc inhibitors have been developed to treat Th17-related autoimmune disorders (Pandya et al., 2018). One could speculate that treatment of iCCA

patients with a high peri-tumoral TLS score with RORc inhibitors might transform these TLSs into anti-tumorigenic ones.

The induction of TLSs may have a great impact on cancer treatment. However, it is not sufficient to induce TLSs but also to control the nature of the TLSs formed, in order to achieve a favorable outcome. Here we show that the deletion of RORc expressing cells resulted in induction of excess TLSs with anti-tumorigenic potential. Future research is needed to discover whether there is a link between the cells and signals that induce TLS formation and the ways they shape the TLS immune composition and phenotype. While immunotherapy with ICBs has revolutionized the treatment of liver cancer, response rates are still low (Llovet et al., 2021). It is thus interesting to speculate that manipulating TLS states could affect responses to ICBs in liver cancer. Additionally, assessing TLS phenotypes in liver cancer could prove to be a valuable biomarker for response to immunotherapy.

Acknowledgments: We thank Shlomi Finkin and Orit Pappo for their help and advice; Fatima Mushasha, Nasrallah Nasrallah, Bareket Ben-Amos, Abdelmajeed Nasereddin, Idit Shiff, Hasan Sourikh, Eleonora Medvedev and Mohammad Jumaa for excellent technical assistance; Tali Bdolah-Abram for help with the statistical analyses.

Author contribution: EC, IS and EP conceived the study. EC and IS designed and carried out most experiments. EC, IS and EP wrote the manuscript. EZ, SR, T-MS and SR-Z helped with additional experiments and data analysis. OP, YS and YS performed the bioinformatics analyses. OP, ML and YB-N provided valuable feedback and insights to the study. All authors read and approved the manuscript.

Funding: This work was supported by grants to EP from the Dr. Miriam and Sheldon G Adelson Medical Research Foundation, the Israel Science Foundation (ISF) and the Cooperation Program in Cancer Research of the Deutsches Krebsforschungszentrum (DKFZ) and Israel's Ministry of Science and Technology (MOST).

Competing Interests: Authors declare no competing interests.

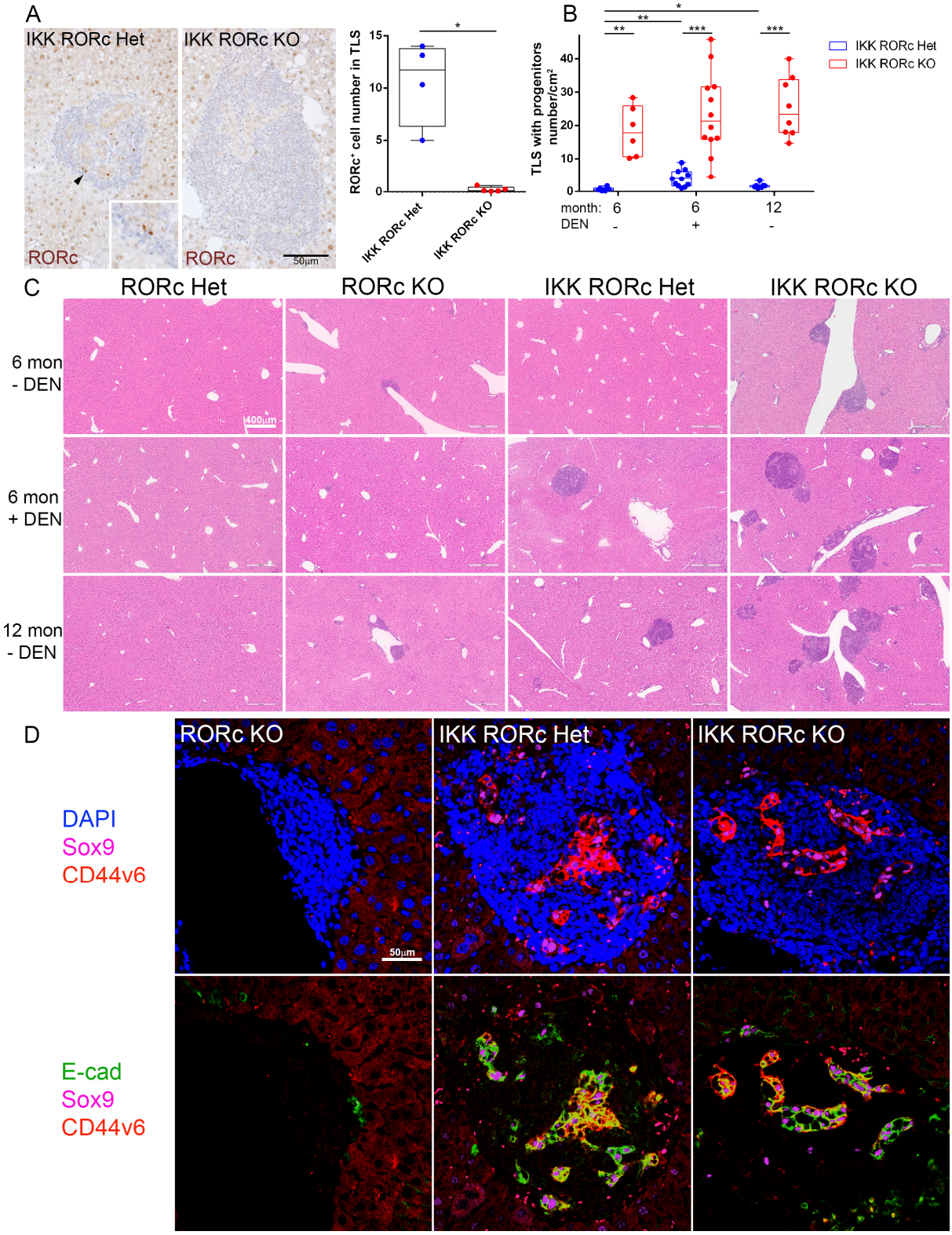

Figure 1: RORc expressing cells are not necessary for liver TLS neogenesis, but rather negatively regulate TLS formation. (A) Representative images of TLSs of DEN-injected 6 months old IKK RORc Het (left) and IKK RORc KO (right) mice immunostained for RORc (scale bar 50µm) and the corresponding quantification (each data point is an average of several

TLSs. For all figures, each data point represents a single mouse). Arrowhead: RORc expressing cells (also shown in the inset). **(B)** Numbers of TLSs with tumor progenitors. **(C)** Representative images of H&E stained liver sections (scale bar 400μm) in spontaneous conditions at 6 months (6 mon – DEN), at 6 months following DEN injection (6 mon + DEN) and in spontaneous conditions at 12 months of age (12 mon – DEN). **(D)** Triple immunofluorescent staining for Sox9, CD44v6 and E-cadherin. DAPI was used as counterstain, and delineates the TLSs. Sox9 (pink, nuclear) and CD44v6 (red, membranous) are tumor progenitor markers. E-cadherin marks all epithelial cells (scale bar 50μm). Note that TLS-like structures in RORc KO mice do not harbor tumor progenitor cells. Statistical tests applied: Mann-Whitney (A); Kruskal-Wallis with Bonferroni correction (B).

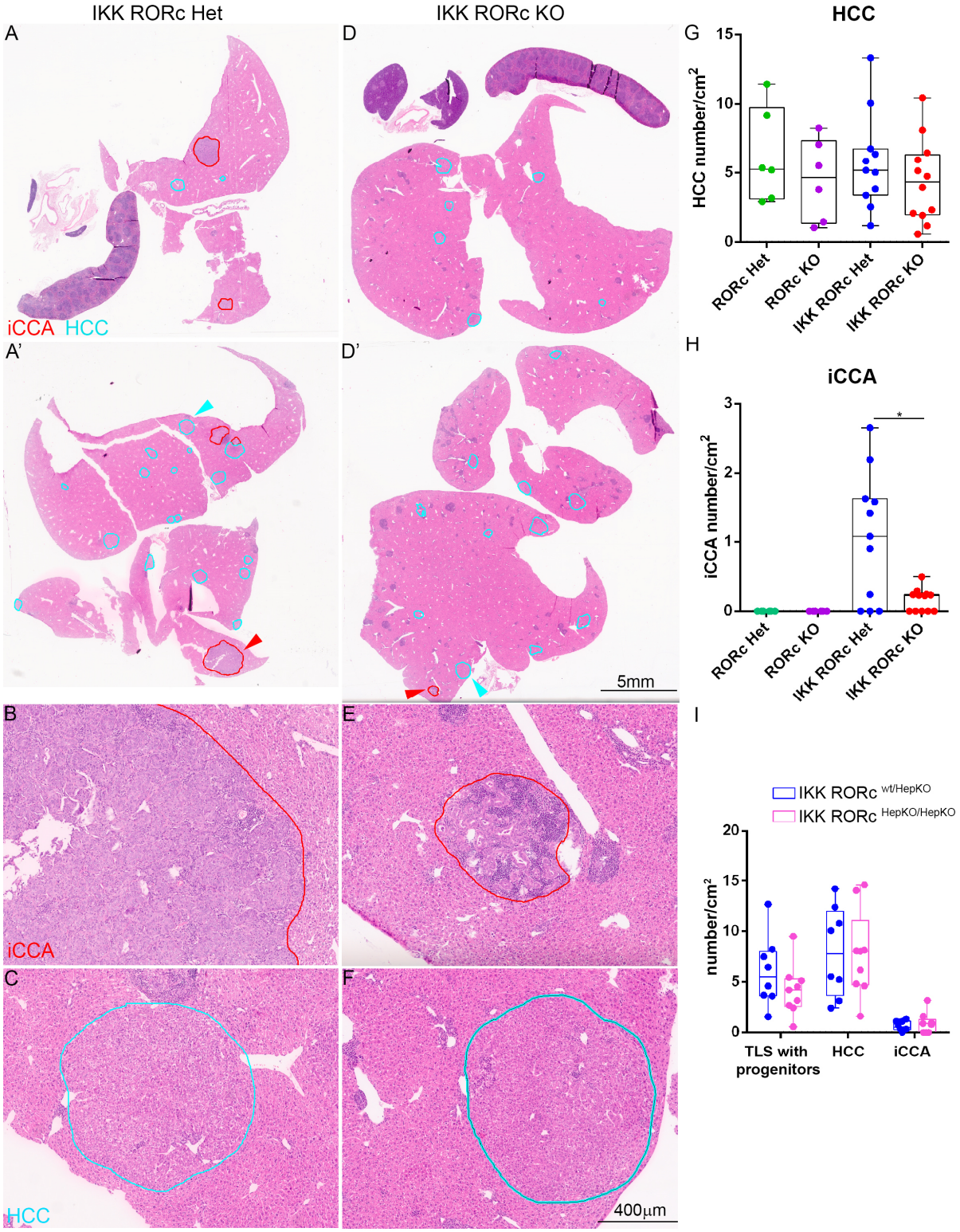

Figure 2: Intrahepatic cholangiocarcinoma (iCCA) but not HCC formation is supported by RORc expressing cells. (A-F) Representative low and high magnification images of H&E stained liver sections. Two sections per mouse, representing the entire liver are shown (A, A' and D, D'). HCCs are circled in light blue and iCCAs in red. Tumors indicated by arrowheads in

A' and D' are shown in higher magnification in B,C and E,F respectively. Scale bar in A, A', D, D' is 5mm and in B,C,E,F 400μm. **(G)** HCC numbers in DEN-injected 6 months old mice. **(H)** iCCA numbers in DEN-injected 6 months old mice. **(I)** TLSs with progenitors, HCC and iCCA numbers in DEN-injected 6 months old IKK $RORc^{wt/HepKO}$ and IKK $RORc^{HepKO/HepKO}$ mice. Statistical tests applied: (G) Kruskal-Wallis with Bonferroni correction; (H) Kruskal-Wallis; (I) Mann-Whitney.

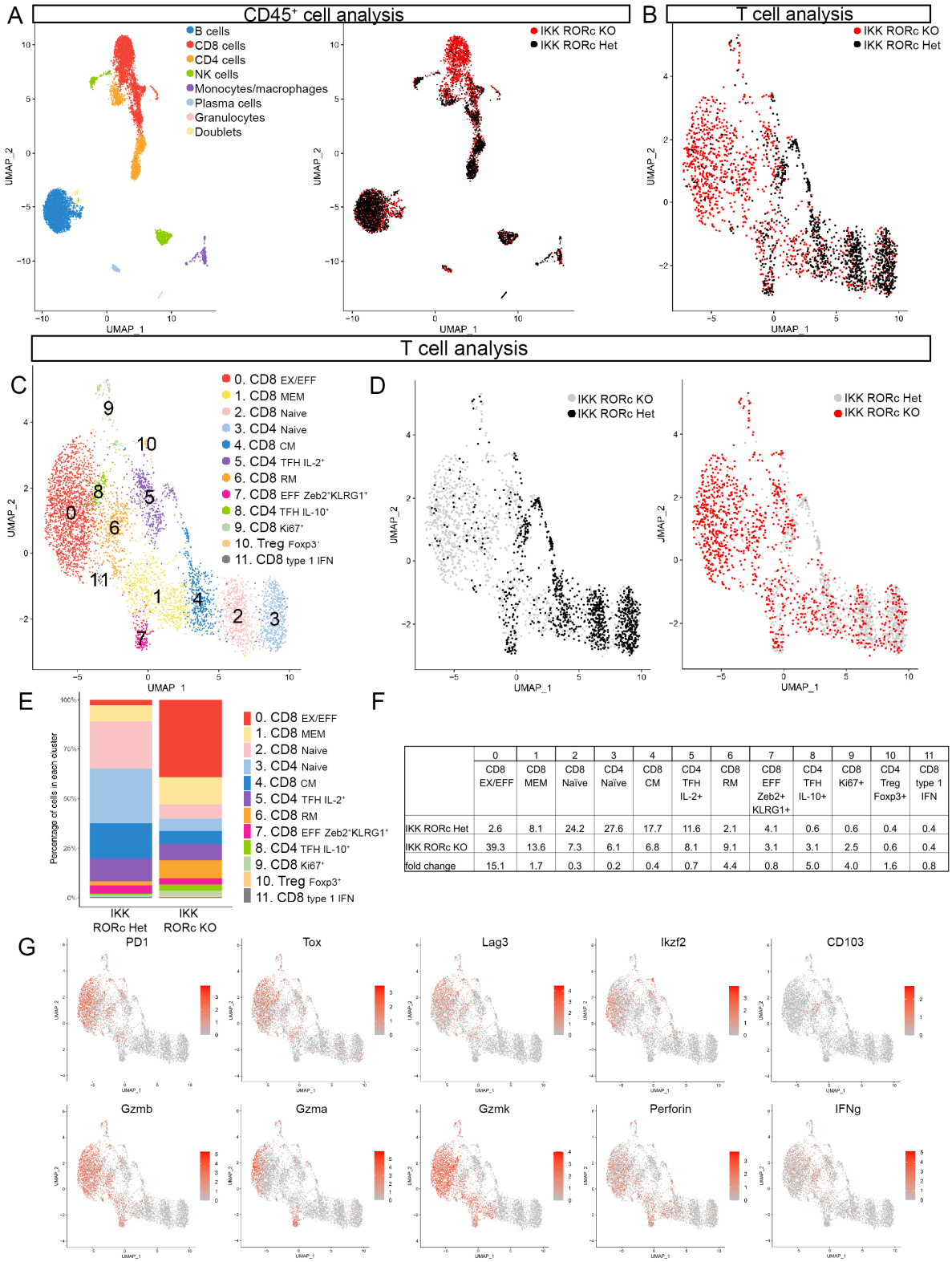

	0	1	2	3	4	5	6	7	8	9	10	11
	CD8 EX/EFF	CD8 MEM	CD8 Naïve	CD4 Naïve	CD8 CM	CD4 TFH IL-2+	CD8 RM	CD8 EFF Zeb2+ KLRG1+	CD4 TFH IL-10+	CD8 Ki67+	CD4 Treg Foxp3+	CD8 type 1 IFN
IKK RORc Het	2.6	8.1	24.2	27.6	17.7	11.6	2.1	4.1	0.6	0.6	0.4	0.4
IKK RORc KO	39.3	13.6	7.3	6.1	6.8	8.1	9.1	3.1	3.1	2.5	0.6	0.4
fold change	15.1	1.7	0.3	0.2	0.4	0.7	4.4	0.8	5.0	4.0	1.6	0.8

Figure 3: Exhausted yet cytotoxic CD8 cells are enriched in IKK RORc KO livers. scRNA-seq analysis of CD45+ cells isolated from livers of DEN-injected 6 months old IKK RORc Het mice (pool of 3 mice) and IKK RORc KO mice (2 mice). **(A)** Uniform manifold approximation and projections (UMAPs) showing the different cell populations (left) and the distribution of cells

between IKK RORc Het (black) and IKK RORc KO (red) (right). **(B-C)** Same as A but restricted to $CD3^+$ cells. T cells cluster identity is shown in (C). **(D)** UMAP depicted in (B) highlighting the T cell distribution of IKK RORc Het (black) on top of IKK RORc KO (gray) (on the left), and IKK RORc KO (red) on top of IKK RORc Het (gray) (on the right). In (B) and (D) the number of cells in IKK RORc KO was randomly down-sampled, in order to show equal numbers of cells from IKK RORc Het and IKK RORc KO. **(E-F)** Diagram and table showing the distribution of cells across clusters in each condition, represented as percentages. Fold change for selected clusters= IKK RORc KO/IKK RORc Het. **(G)** Expression of indicated genes on the UMAP of the T cell analysis (high expression levels – red, low expression levels – gray). Abbreviations: $CD8_{EX/EFF}$-CD8 exhausted/effector, $CD8_{EFF}$-CD8 effector, $CD8_{MEM}$-CD8 memory, $CD8_{CM}$-CD8 central memory, $CD4_{TFH}$-CD4 T follicular helper, $CD8_{RM}$-CD8 resident memory, T_{REG}-T regulatory.

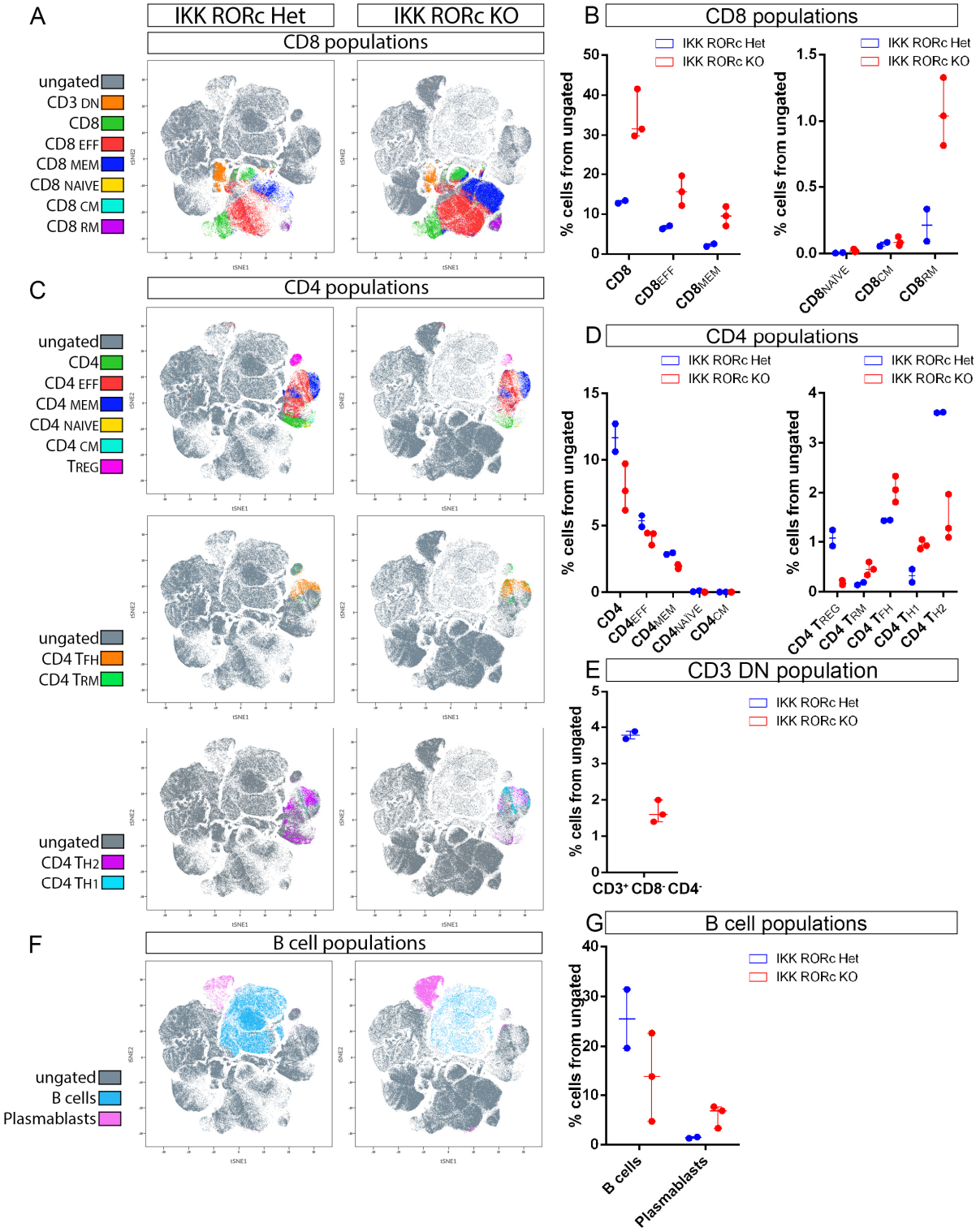

Figure 4: CyTOF analysis reveals enrichment of effector and memory CD8 cells and shift from T_{H2} to T_{H1} phenotype of CD4 cells in IKK RORc KO livers. Immune cells were isolated from livers of DEN-injected 6 months old control mice (n=2, each representing a pool of 3 IKK RORc Het or 4 IKK mice) and IKK RORc KO mice (n=3, each from a single mouse) and analyzed using

CyTOF. **(A)** tSNE plots highlighting CD8 cells. **(B)** Percentages of CD8 cell subsets from the ungated population in IKK RORc Het compared to IKK RORc KO. $CD8_{EFF}$ ($CD44^+$ $CD262L^-$ $CCR7^-$ $IL7Ra^-$), $CD8_{MEM}$ ($CD44^+$ $CD262L^-$ $CCR7^-$ $IL7Ra^+$) and $CD8_{RM}$ ($CD103^+CD69^+$) are increased in IKK RORc KO. **(C)** tSNE plots highlighting CD4 cells. **(D)** Percentages of CD4 cell subsets from the ungated population in IKK RORc Het compared to IKK RORc KO. $CD4_{RM}$ ($CD103^+CD69^+$), CD4 T_{FH} ($ICOS^+$), CD4 T_{H1} ($Tbet^+$) are increased while Tregs ($Foxp3^+$) and CD4 T_{H2} ($Gata3^+$) are decreased in IKK RORc KO. **(E)** Percentages of $CD3^+$ $CD8^-$ $CD4^-$ double negative (DN) cells are decreased in IKK RORc KO ($CD3_{DN}$ cluster is shown in the tSNE in panel A). **(F,G)** B cells ($CD19^+$) and plasmablasts ($CD19^{-/+}$ $IRF4^+$ $Ki67^+$) populations and their percentages. Abbreviations: $CD3_{DN}$-CD3 double negative, $CD8_{EFF}$-CD8 effector, $CD8_{MEM}$-CD8 memory, $CD8_{CM}$-CD8 central memory, $CD8_{RM}$-CD8 resident memory, $CD4_{EFF}$-CD4 effector, $CD4_{MEM}$-CD4 memory, $CD4_{CM}$-CD4 central memory, $CD4_{RM}$-CD4 resident memory, $CD4_{TFH}$-CD4 T follicular helper, T_{REG}-T regulatory, T_{H1}-T helper 1, T_{H2}-T helper 2.

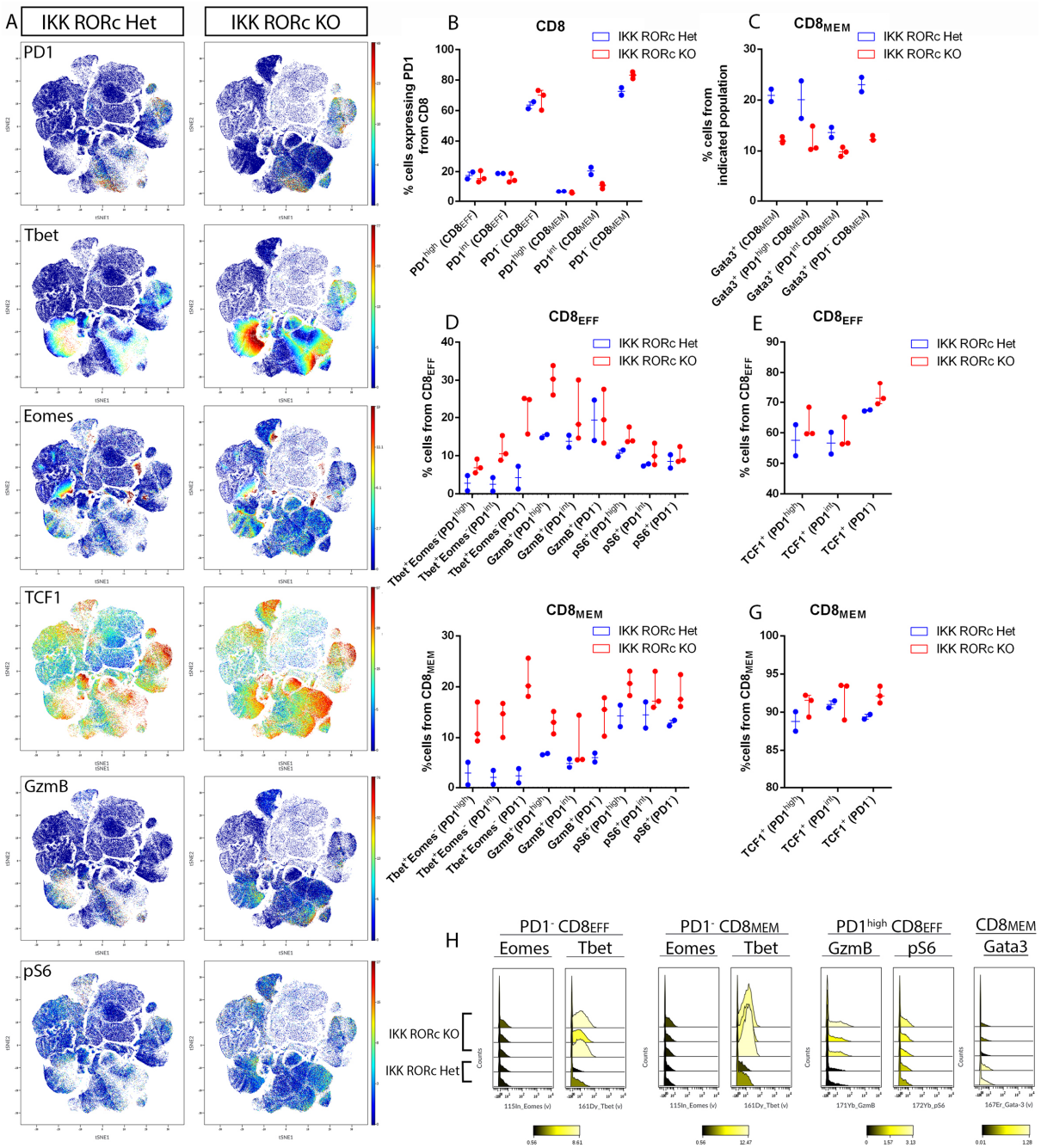

Figure 5: RORc⁺ cells restrict CD8 effector and memory cells with a progenitor phenotype. Same experiment shown in Fig. 4. **(A)** Expression of indicated genes on tSNE plots (high expression level - red, low expression level - blue). **(B-G)** Comparisons of specific cell percentages. Note that the denominator population is different in different graphs as indicated. **(H)** Histograms of cell counts as a function of signal intensity in IKK RORc Het (2 lower histograms) vs. IKK RORc KO (3 upper histograms) for Eomes and Tbet in the PD1⁻ expressing $CD8_{EFF}$ and $CD8_{MEM}$ populations. GzmB and pS6 expression intensity are shown in

the PD1^{high} CD8$_{EFF}$ population and Gata3 expression intensity is shown in the CD8$_{MEM}$ population (high expression level - yellow, low expression level - black).

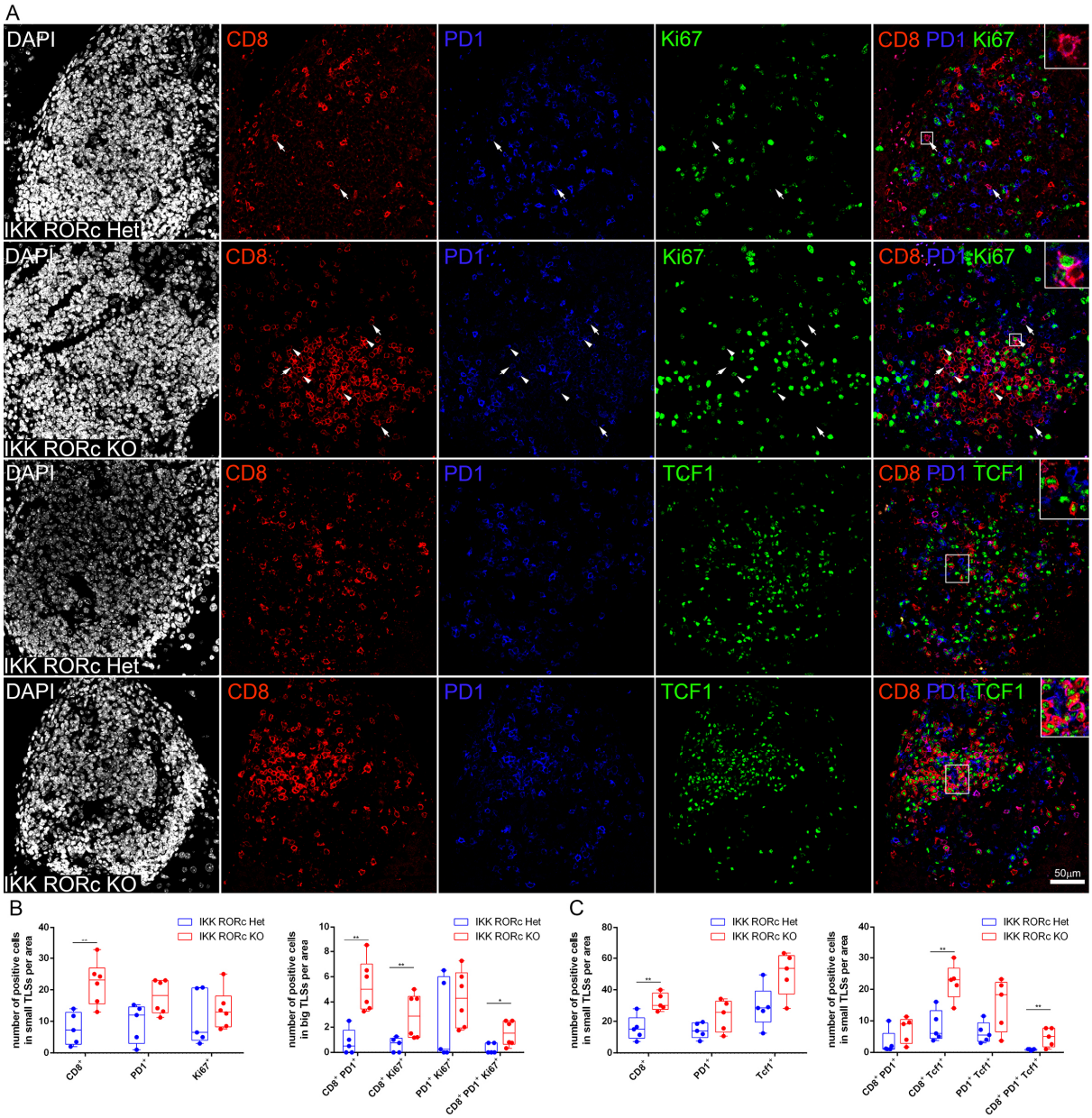

Figure 6: Proliferating and progenitor-like CD8 cells expressing PD1, are enriched within TLSs of IKK RORc KO. (A) Representative triple immunostaining for the indicated markers in TLSs of IKK RORc Het and IKK RORc KO mice. In the two upper panels, arrows point to CD8$^+$ PD1$^+$ cells and arrowheads point to CD8$^+$ PD1$^+$ Ki67$^+$ cells. Cells co-expressing CD8 (red) and PD1 (blue) are seen in pink. Insets correspond to areas in white boxes (scale bar 50µm). **(B)** Numbers of cells expressing CD8, PD1 or Ki67 (left) and their combinations (right) within TLSs.

(C) Numbers of cells expressing CD8, PD1 or TCF1 (left) and their combinations (right) in TLSs. Statistical test applied: Mann-Whitney.

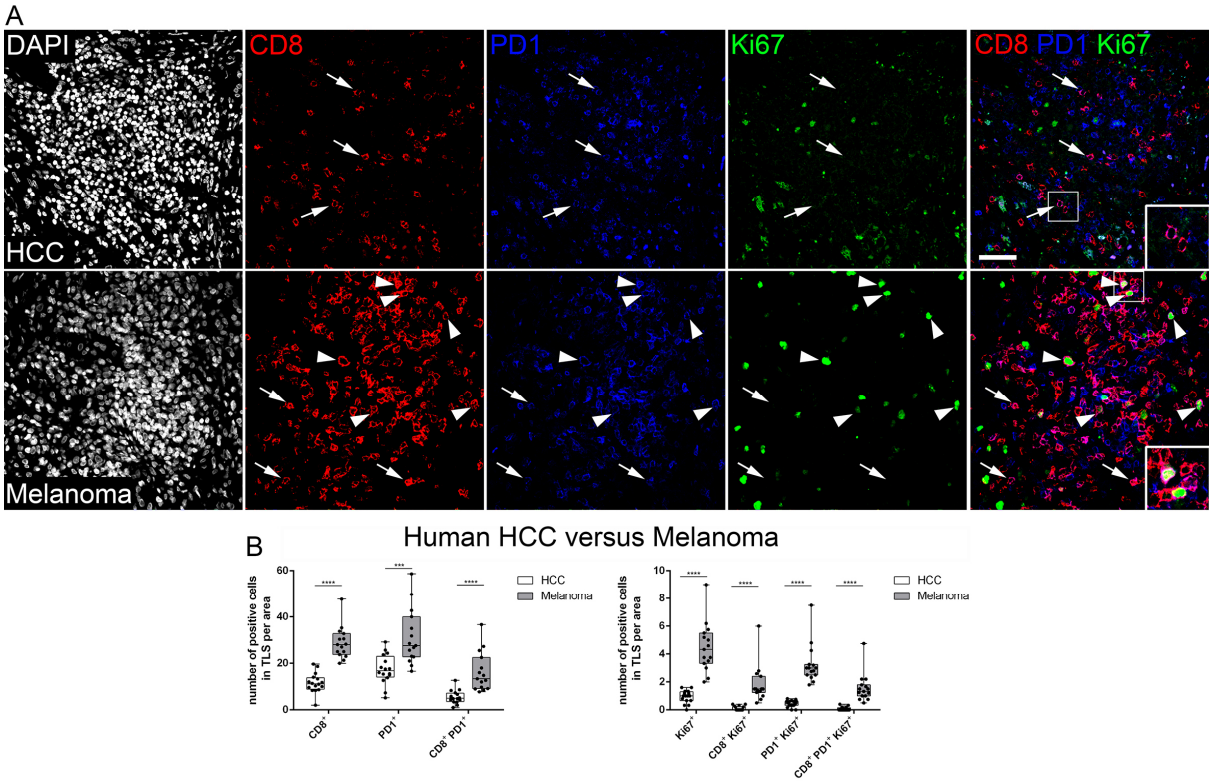

Figure 7: CD8 cells with an exhausted yet proliferative state are enriched in TLSs in Melanoma patients compared to TLSs in HCC patients. (A) Representative pictures of triple immunostaining of TLS in peritumor area of HCC (upper panel) and melanoma (lower panel). Arrows point to $CD8^+$ $PD1^+$ cells, and arrowheads point to $CD8^+$ $PD1^+$ $Ki67^+$ cells. Insets correspond to areas in white boxes (scale bar 50μm). **(B)** Numbers of cells expressing CD8, PD1 or Ki67 and their combinations within TLSs in HCC and melanoma. Statistical test applied: Mann-Whitney.

References

Beltra, J. C., Manne, S., Abdel-Hakeem, M. S., Kurachi, M., Giles, J. R., Chen, Z., Casella, V., Ngiow, S. F., Khan, O., Huang, Y. J., Yan, P., Nzingha, K., Xu, W., Amaravadi, R. K., Xu, X., Karakousis, G. C., Mitchell, T. C., Schuchter, L. M., Huang, A. C., & Wherry, E. J. (2020). Developmental Relationships of Four Exhausted CD8+ T Cell Subsets Reveals Underlying Transcriptional and Epigenetic Landscape Control Mechanisms. *Immunity*, *52*(5), 825-

841.e8. https://doi.org/10.1016/J.IMMUNI.2020.04.014

Bertuccio, P., Malvezzi, M., Carioli, G., Hashim, D., Boffetta, P., El-Serag, H. B., La Vecchia, C., & Negri, E. (2019). Global trends in mortality from intrahepatic and extrahepatic cholangiocarcinoma. *Journal of Hepatology*, *71*(1), 104–114. https://doi.org/10.1016/J.JHEP.2019.03.013

Cabrita, R., Lauss, M., Sanna, A., Donia, M., Skaarup Larsen, M., Mitra, S., Johansson, I., Phung, B., Harbst, K., Vallon-Christersson, J., van Schoiack, A., Lövgren, K., Warren, S., Jirström, K., Olsson, H., Pietras, K., Ingvar, C., Isaksson, K., Schadendorf, D., … Jönsson, G. (2020). Tertiary lymphoid structures improve immunotherapy and survival in melanoma. *Nature 2020 577:7791*, *577*(7791), 561–565. https://doi.org/10.1038/s41586-019-1914-8

Calderaro, J., Petitprez, F., Becht, E., Laurent, A., Hirsch, T. Z., Rousseau, B., Luciani, A., Amaddeo, G., Derman, J., Charpy, C., Zucman-Rossi, J., Fridman, W. H., & Sautès-Fridman, C. (2019). Intra-tumoral tertiary lymphoid structures are associated with a low risk of early recurrence of hepatocellular carcinoma. *Journal of Hepatology*, *70*(1), 58–65. https://doi.org/10.1016/J.JHEP.2018.09.003

Carrega, P., Loiacono, F., Carlo, E. Di, Scaramuccia, A., Mora, M., Conte, R., Benelli, R., Spaggiari, G. M., Cantoni, C., Campana, S., Bonaccorsi, I., Morandi, B., Truini, M., Mingari, M. C., Moretta, L., & Ferlazzo, G. (2015). ARTICLE NCR þ ILC3 concentrate in human lung cancer and associate with intratumoral lymphoid structures. *Nature Communications*. https://doi.org/10.1038/ncomms9280

Chaurio, R. A., Anadon, C. M., Lee Costich, T., Payne, K. K., Biswas, S., Harro, C. M., Moran, C., Ortiz, A. C., Cortina, C., Rigolizzo, K. E., Sprenger, K. B., Mine, J. A., Innamarato, P., Mandal, G., Powers, J. J., Martin, A., Wang, Z., Mehta, S., Perez, B. A., … Conejo-Garcia, J. R. (2022). TGF-β-mediated silencing of genomic organizer SATB1 promotes Tfh cell differentiation and formation of intra-tumoral tertiary lymphoid structures. *Immunity*, *55*(1), 115-128.e9. https://doi.org/10.1016/J.IMMUNI.2021.12.007

Chew, V., Chen, J., Lee, D., Loh, E., Lee, J., Lim, K. H., Weber, A., Slankamenac, K., Poon, R. T. P., Yang, H., Ooi, L. L. P. J., Toh, H. C., Heikenwalder, M., Ng, I. O. L., Nardin, A., &

Abastado, J. P. (2012). Chemokine-driven lymphocyte infiltration: an early intratumoural event determining long-term survival in resectable hepatocellular carcinoma. *Gut*, *61*(3), 427–438. https://doi.org/10.1136/GUTJNL-2011-300509

Chew, V., Lai, L., Pan, L., Lim, C. J., Li, J., Ong, R., Chua, C., Leong, J. Y., Lim, K. H., Toh, H. C., Lee, S. Y., Chan, C. Y., Goh, B. K. P., Chung, A., Chow, P. K. H., & Albani, S. (2017). Delineation of an immunosuppressive gradient in hepatocellular carcinoma using high-dimensional proteomic and transcriptomic analyses. *Proceedings of the National Academy of Sciences of the United States of America*, *114*(29), E5900–E5909. https://doi.org/10.1073/PNAS.1706559114/SUPPL_FILE/PNAS.1706559114.SAPP.PDF

Couper, K. N., Blount, D. G., Wilson, M. S., Hafalla, J. C., Belkaid, Y., Kamanaka, M., Flavell, R. A., De Souza, J. B., & Riley, E. M. (2008). IL-10 from CD4CD25Foxp3CD127 adaptive regulatory T cells modulates parasite clearance and pathology during malaria infection. *PLoS Pathogens*, *4*(2). https://doi.org/10.1371/JOURNAL.PPAT.1000004

Ding, G. Y., Ma, J. Q., Yun, J. P., Chen, X., Ling, Y., Zhang, S., Shi, J. Y., Chang, Y. Q., Ji, Y., Wang, X. Y., Tan, W. M., Yuan, K. F., Yan, B., Zhang, X. M., Liang, F., Zhou, J., Fan, J., Zeng, Y., Cai, M. Y., & Gao, Q. (2022). Distribution and density of tertiary lymphoid structures predict clinical outcome in intrahepatic cholangiocarcinoma. *Journal of Hepatology*, *76*(3), 608–618. https://doi.org/10.1016/J.JHEP.2021.10.030

Eberl, G. (2017). RORγt, a multitask nuclear receptor at mucosal surfaces. *Mucosal Immunology*, *10*(1), 27–34. https://doi.org/10.1038/mi.2016.86

Eberl, G., Marmon, S., Sunshine, M. J., Rennert, P. D., Choi, Y., & Littmann, D. R. (2004). An essential function for the nuclear receptor RORγt in the generation of fetal lymphoid tissue inducer cells. *Nature Immunology*, *5*(1), 64–73. https://doi.org/10.1038/ni1022

Figenschau, S. L., Fismen, S., Fenton, K. A., Fenton, C., & Mortensen, E. S. (2015). Tertiary lymphoid structures are associated with higher tumor grade in primary operable breast cancer patients. *BMC Cancer*, *15*, 101. https://doi.org/10.1186/s12885-015-1116-1

Finkin, S., Yuan, D., Stein, I., Taniguchi, K., Weber, A., Unger, K., Browning, J. L., Goossens, N., Nakagawa, S., Gunasekaran, G., Schwartz, M. E., Kobayashi, M., Kumada, H., Berger, M., Pappo, O., Rajewsky, K., Hoshida, Y., Karin, M., Heikenwalder, M., … Pikarsky, E.

(2015). Ectopic lymphoid structures function as microniches for tumor progenitor cells in hepatocellular carcinoma. *Nature Immunology*, *16*(12), 1235–1244. https://doi.org/10.1038/ni.3290

Griss, J., Bauer, W., Wagner, C., Simon, M., Chen, M., Grabmeier-Pfistershammer, K., Maurer-Granofszky, M., Roka, F., Penz, T., Bock, C., Zhang, G., Herlyn, M., Glatz, K., Läubli, H., Mertz, K. D., Petzelbauer, P., Wiesner, T., Hartl, M., Pickl, W. F., … Wagner, S. N. (2019). B cells sustain inflammation and predict response to immune checkpoint blockade in human melanoma. *Nature Communications*, *10*(1). https://doi.org/10.1038/s41467-019-12160-2

Hamilton, D. H., & Bretscher, P. A. (2008). Different immune correlates associated with tumor progression and regression: Implications for prevention and treatment of cancer. *Cancer Immunology, Immunotherapy*, *57*(8), 1125–1136. https://doi.org/10.1007/S00262-007-0442-9/FIGURES/7

Hao, Y., Hao, S., Andersen-Nissen, E., Mauck, W. M., Zheng, S., Butler, A., Lee, M. J., Wilk, A. J., Darby, C., Zager, M., Hoffman, P., Stoeckius, M., Papalexi, E., Mimitou, E. P., Jain, J., Srivastava, A., Stuart, T., Fleming, L. M., Yeung, B., … Satija, R. (2021). Integrated analysis of multimodal single-cell data. *Cell*, *184*(13), 3573-3587.e29. https://doi.org/10.1016/J.CELL.2021.04.048

Häringer, B., Lozza, L., Steckel, B., & Geginat, J. (2009). Identification and characterization of IL-10/IFN-γ–producing effector-like T cells with regulatory function in human blood. *Journal of Experimental Medicine*, *206*(5), 1009–1017. https://doi.org/10.1084/JEM.20082238

Helmink, B. A., Reddy, S. M., Gao, J., Zhang, S., Basar, R., Thakur, R., Yizhak, K., Sade-Feldman, M., Blando, J., Han, G., Gopalakrishnan, V., Xi, Y., Zhao, H., Amaria, R. N., Tawbi, H. A., Cogdill, A. P., Liu, W., LeBleu, V. S., Kugeratski, F. G., … Wargo, J. A. (2020). B cells and tertiary lymphoid structures promote immunotherapy response. *Nature*. https://doi.org/10.1038/s41586-019-1922-8

Huang, A. C., Postow, M. A., Orlowski, R. J., Mick, R., Bengsch, B., Manne, S., Xu, W., Harmon, S., Giles, J. R., Wenz, B., Adamow, M., Kuk, D., Panageas, K. S., Carrera, C.,

Wong, P., Quagliarello, F., Wubbenhorst, B., D'Andrea, K., Pauken, K. E., … Wherry, E. J. (2017). T-cell invigoration to tumour burden ratio associated with anti-PD-1 response. *Nature*, *545*(7652), 60–65. https://doi.org/10.1038/nature22079

Huang, Y., Liang, H., He, C., Peng, F., & Hu, G. (2019). Hepatitis B Virus X Protein-Induced ROR γ Expression to Promote the Migration and Proliferation of Hepatocellular Carcinoma. *BioMed Research International*, *2019*. https://doi.org/10.1155/2019/5407126

Hutloff, A. (2018). T Follicular Helper-Like Cells in Inflamed Non-Lymphoid Tissues. *Frontiers in Immunology*, *9*, 1707. https://doi.org/10.3389/fimmu.2018.01707

Joshi, N. S., Akama-Garren, E. H., Lu, Y., Lee, D.-Y., Chang, G. P., Li, A., DuPage, M., Tammela, T., Kerper, N. R., Farago, A. F., Robbins, R., Crowley, D. M., Bronson, R. T., & Jacks, T. (2015). Regulatory T Cells in Tumor-Associated Tertiary Lymphoid Structures Suppress Anti-tumor T Cell Responses. *Immunity*, *43*(3), 579–590. https://doi.org/10.1016/j.immuni.2015.08.006

Kim, H. D., Song, G. W., Park, S., Jung, M. K., Kim, M. H., Kang, H. J., Yoo, C., Yi, K., Kim, K. H., Eo, S., Moon, D. B., Hong, S. M., Ju, Y. S., Shin, E. C., Hwang, S., & Park, S. H. (2018). Association Between Expression Level of PD1 by Tumor-Infiltrating CD8+ T Cells and Features of Hepatocellular Carcinoma. *Gastroenterology*, *155*(6), 1936-1950.e17. https://doi.org/10.1053/j.gastro.2018.08.030

Kuen, D. S., Kim, B. S., & Chung, Y. (2020). IL-17-Producing Cells in Tumor Immunity: Friends or Foes? *Immune Network*, *20*(1). https://doi.org/10.4110/IN.2020.20.E6

Kumar, P., Saini, S., & Prabhakar, B. S. (2019). Cancer immunotherapy with check point inhibitor can cause autoimmune adverse events due to loss of Treg homeostasis. *Seminars in Cancer Biology*. https://doi.org/10.1016/J.SEMCANCER.2019.01.006

Kurtulus, S., Madi, A., Escobar, G., Klapholz, M., Nyman, J., Christian, E., Pawlak, M., Dionne, D., Xia, J., Rozenblatt-Rosen, O., Kuchroo, V. K., Regev, A., & Anderson, A. C. (2019). Checkpoint Blockade Immunotherapy Induces Dynamic Changes in PD-1–CD8+ Tumor-Infiltrating T Cells. *Immunity*, *50*(1), 181-194.e6. https://doi.org/10.1016/J.IMMUNI.2018.11.014

Liu, Y., Song, Y., Lin, D., Lei, L., Mei, Y., Jin, Z., Gong, H., Zhu, Y., Hu, B., Zhang, Y., Zhao, L., Teo, H. Y., Qiu, J., Jiang, W., Dong, C., Wu, D., Huang, Y., & Liu, H. (2019). NCR – group 3 innate lymphoid cells orchestrate IL-23/IL-17 axis to promote hepatocellular carcinoma development. *EBioMedicine*, *41*, 333–344. https://doi.org/10.1016/j.ebiom.2019.02.050

Llovet, J. M., Castet, F., Heikenwalder, M., Maini, M. K., Mazzaferro, V., Pinato, D. J., Pikarsky, E., Zhu, A. X., & Finn, R. S. (2021). Immunotherapies for hepatocellular carcinoma. *Nature Reviews Clinical Oncology 2021 19:3*, *19*(3), 151–172. https://doi.org/10.1038/s41571-021-00573-2

Lochner, M., Ohnmacht, C., Presley, L., Bruhns, P., Si-Tahar, M., Sawa, S., & Eberl, G. (2011). Microbiota-induced tertiary lymphoid tissues aggravate inflammatory disease in the absence of RORgamma t and LTi cells. *The Journal of Experimental Medicine*, *208*(1), 125–134. https://doi.org/10.1084/jem.20100052

Ma, S., Cheng, Q., Cai, Y., Gong, H., Wu, Y., Yu, X., Shi, L., Wu, D., Dong, C., & Liu, H. (2014). IL-17A produced by γδ T cells promotes tumor growth in hepatocellular carcinoma. *Cancer Research*, *74*(7), 1969–1982. https://doi.org/10.1158/0008-5472.CAN-13-2534/651148/AM/IL-17A-PRODUCED-BY-T-CELLS-PROMOTES-TUMOR-GROWTH

Marinkovic, T., Garin, A., Yokota, Y., Fu, Y.-X., Ruddle, N. H., Furtado, G. C., & Lira, S. A. (2006). Interaction of mature CD3+CD4+ T cells with dendritic cells triggers the development of tertiary lymphoid structures in the thyroid. *The Journal of Clinical Investigation*, *116*(10), 2622–2632. https://doi.org/10.1172/JCI28993

Messina, J. L., Fenstermacher, D. A., Eschrich, S., Qu, X., Berglund, A. E., Lloyd, M. C., Schell, M. J., Sondak, V. K., Weber, J. S., & Mulé, J. J. (2012). 12-Chemokine gene signature identifies lymph node-like structures in melanoma: potential for patient selection for immunotherapy? *Scientific Reports*, *2*. https://doi.org/10.1038/SREP00765

Meylan, M., Petitprez, F., Lacroix, L., Tommaso, L. Di, Roncalli, M., Bougouin, A., Laurent, A., Amaddeo, G., Sommacale, D., Regnault, H., Derman, J., Charpy, C., Lafdil, F., Pawlotsky, J. M., Sautes-Fridman, C., Fridman, W. H., & Calderaro, J. (2020). Early Hepatic Lesions Display Immature Tertiary Lymphoid Structures and Show Elevated Expression of

Immune Inhibitory and Immunosuppressive Molecules. *Clinical Cancer Research*, *26*(16), 4381–4389. https://doi.org/10.1158/1078-0432.CCR-19-2929/77014/AM/EARLY-HEPATIC-LESIONS-DISPLAY-IMMATURE-TERTIARY

Miller, B. C., Sen, D. R., Al Abosy, R., Bi, K., Virkud, Y. V., LaFleur, M. W., Yates, K. B., Lako, A., Felt, K., Naik, G. S., Manos, M., Gjini, E., Kuchroo, J. R., Ishizuka, J. J., Collier, J. L., Griffin, G. K., Maleri, S., Comstock, D. E., Weiss, S. A., … Haining, W. N. (2019). Subsets of exhausted CD8+ T cells differentially mediate tumor control and respond to checkpoint blockade. *Nature Immunology*, *20*(3), 326–336. https://doi.org/10.1038/s41590-019-0312-6

Paley, M. A., Kroy, D. C., Odorizzi, P. M., Johnnidis, J. B., Dolfi, D. V., Barnett, B. E., Bikoff, E. K., Robertson, E. J., Lauer, G. M., Reiner, S. L., & Wherry, E. J. (2012). Progenitor and terminal subsets of CD8+ T cells cooperate to contain chronic viral infection. *Science*, *338*(6111), 1220–1225. https://doi.org/10.1126/science.1229620

Pandya, V. B., Kumar, S., Sachchidanand, Sharma, R., & Desai, R. C. (2018). Combating Autoimmune Diseases with Retinoic Acid Receptor-Related Orphan Receptor-γ (RORγ or RORc) Inhibitors: Hits and Misses. *Journal of Medicinal Chemistry*, *61*(24), 10976–10995. https://doi.org/10.1021/ACS.JMEDCHEM.8B00588/ASSET/IMAGES/LARGE/JM-2018-00588N_0011.JPEG

Pauken, K. E., & Wherry, E. J. (2015). Overcoming T cell exhaustion in infection and cancer. In *Trends in Immunology* (Vol. 36, Issue 4, pp. 265–276). Elsevier Ltd. https://doi.org/10.1016/j.it.2015.02.008

Peske, J. D., Thompson, E. D., Gemta, L., Baylis, R. A., Fu, Y. X., & Engelhard, V. H. (2015). Effector lymphocyte-induced lymph node-like vasculature enables naive T-cell entry into tumours and enhanced anti-tumour immunity. *Nature Communications 2015 6:1*, *6*(1), 1–15. https://doi.org/10.1038/ncomms8114

Petitprez, F., de Reyniès, A., Keung, E. Z., Chen, T. W.-W., Sun, C.-M., Calderaro, J., Jeng, Y.-M., Hsiao, L.-P., Lacroix, L., Bougoüin, A., Moreira, M., Lacroix, G., Natario, I., Adam, J., Lucchesi, C., Laizet, Y. H., Toulmonde, M., Burgess, M. A., Bolejack, V., … Fridman, W. H. (2020). B cells are associated with survival and immunotherapy response in sarcoma.

Nature. https://doi.org/10.1038/s41586-019-1906-8

Pikor, N. B., Astarita, J. L., Summers-Deluca, L., Galicia, G., Qu, J., Ward, L. A., Armstrong, S., Dominguez, C. X., Malhotra, D., Heiden, B., Kay, R., Castanov, V., Touil, H., Boon, L., O'Connor, P., Bar-Or, A., Prat, A., Ramaglia, V., Ludwin, S., … Gommerman, J. L. (2015). Integration of Th17- and Lymphotoxin-Derived Signals Initiates Meningeal-Resident Stromal Cell Remodeling to Propagate Neuroinflammation. *Immunity*, *43*(6), 1160–1173. https://doi.org/10.1016/J.IMMUNI.2015.11.010

Rangel-Moreno, J., Carragher, D. M., De La Luz Garcia-Hernandez, M., Hwang, J. Y., Kusser, K., Hartson, L., Kolls, J. K., Khader, S. A., & Randall, T. D. (2011). The development of inducible bronchus-associated lymphoid tissue depends on IL-17. *Nature Immunology*, *12*(7), 639–646. https://doi.org/10.1038/ni.2053

Rodriguez, A. B., Peske, J. D., Woods, A. N., Leick, K. M., Mauldin, I. S., Meneveau, M. O., Young, S. J., Lindsay, R. S., Melssen, M. M., Cyranowski, S., Parriott, G., Conaway, M. R., Fu, Y. X., Slingluff, C. L., & Engelhard, V. H. (2021). Immune mechanisms orchestrate tertiary lymphoid structures in tumors via cancer-associated fibroblasts. *Cell Reports*, *36*(3), 109422. https://doi.org/10.1016/J.CELREP.2021.109422

Sade-Feldman, M., Yizhak, K., Bjorgaard, S. L., Ray, J. P., de Boer, C. G., Jenkins, R. W., Lieb, D. J., Chen, J. H., Frederick, D. T., Barzily-Rokni, M., Freeman, S. S., Reuben, A., Hoover, P. J., Villani, A. C., Ivanova, E., Portell, A., Lizotte, P. H., Aref, A. R., Eliane, J. P., … Hacohen, N. (2018). Defining T Cell States Associated with Response to Checkpoint Immunotherapy in Melanoma. *Cell*, *175*(4), 998-1013.e20. https://doi.org/10.1016/j.cell.2018.10.038

Sasaki, Y., Derudder, E., Hobeika, E., Pelanda, R., Reth, M., Rajewsky, K., & Schmidt-Supprian, M. (2006). Canonical NF-κB Activity, Dispensable for B Cell Development, Replaces BAFF-Receptor Signals and Promotes B Cell Proliferation upon Activation. *Immunity*, *24*(6), 729–739. https://doi.org/10.1016/J.IMMUNI.2006.04.005

Sautès-Fridman, C., Petitprez, F., Calderaro, J., & Fridman, W. H. (2019). Tertiary lymphoid structures in the era of cancer immunotherapy. *Nature Reviews Cancer*, *19*(6), 307–325. https://doi.org/10.1038/s41568-019-0144-6

Schumacher, T. N., & Thommen, D. S. (2022). Tertiary lymphoid structures in cancer. *Science*, *375*(6576). https://doi.org/10.1126/SCIENCE.ABF9419/ASSET/B44E9511-03AD-436A-89A0-110BDC25E3A7/ASSETS/IMAGES/LARGE/SCIENCE.ABF9419-F3.JPG

Siddiqui, I., Schaeuble, K., Chennupati, V., Fuertes Marraco, S. A., Calderon-Copete, S., Pais Ferreira, D., Carmona, S. J., Scarpellino, L., Gfeller, D., Pradervand, S., Luther, S. A., Speiser, D. E., & Held, W. (2019). Intratumoral Tcf1 + PD-1 + CD8 + T Cells with Stem-like Properties Promote Tumor Control in Response to Vaccination and Checkpoint Blockade Immunotherapy. *Immunity*, *50*(1), 195-211.e10. https://doi.org/10.1016/j.immuni.2018.12.021

Singer, M., Wang, C., Cong, L., Marjanovic, N. D., Kowalczyk, M. S., Zhang, H., Nyman, J., Sakuishi, K., Kurtulus, S., Gennert, D., Xia, J., Kwon, J. Y. H., Nevin, J., Herbst, R. H., Yanai, I., Rozenblatt-Rosen, O., Kuchroo, V. K., Regev, A., & Anderson, A. C. (2016). A distinct gene module for dysfunction uncoupled from activation in tumor-infiltrating T cells. *Cell*, *166*(6), 1500. https://doi.org/10.1016/J.CELL.2016.08.052

Tellier, J., & Nutt, S. L. (2017). Standing out from the crowd: How to identify plasma cells. *European Journal of Immunology*, *47*(8), 1276–1279. https://doi.org/10.1002/eji.201747168

Tolba, R., Kraus, T., Liedtke, C., Schwarz, M., & Weiskirchen, R. (2015). Diethylnitrosamine (DEN)-induced carcinogenic liver injury in mice. *Laboratory Animals*, *49*(S1), 59–69. https://doi.org/10.1177/0023677215570086

Tsuji, M., Suzuki, K., Kitamura, H., Maruya, M., Kinoshita, K., Ivanov, I. I., Itoh, K., Littman, D. R., & Fagarasan, S. (2008). Requirement for Lymphoid Tissue-Inducer Cells in Isolated Follicle Formation and T Cell-Independent Immunoglobulin A Generation in the Gut. *Immunity*, *29*(2), 261–271. https://doi.org/10.1016/J.IMMUNI.2008.05.014

Ueda, E., Kurebayashi, S., Sakaue, M., Backlund, M., Koller, B., & Jetten, A. M. (2002). High incidence of T-cell lymphomas in mice deficient in the retinoid-related orphan receptor RORγ. *Cancer Research*, *62*(3), 901–909.

Wichner, K., Fischer, A., Winter, S., Tetzlaff, S., Heimesaat, M. M., Bereswill, S., Rehm, A., Lipp, M., & Höpken, U. E. (2013). *Transition from an autoimmune-prone state to fatal*

autoimmune disease in CCR7 and RORγt double-deficient mice is dependent on gut microbiota. https://doi.org/10.1016/j.jaut.2013.08.007

Workel, H. H., Lubbers, J. M., Arnold, R., Prins, T. M., van der Vlies, P., de Lange, K., Bosse, T., van Gool, I. C., Eggink, F. A., Wouters, M. C. A., Komdeur, F. L., van der Slikke, E. C., Creutzberg, C. L., Kol, A., Plat, A., Glaire, M., Church, D. N., Nijman, H. W., & de Bruyn, M. (2019). A Transcriptionally Distinct CXCL13 + CD103 + CD8 + T-cell Population Is Associated with B-cell Recruitment and Neoantigen Load in Human Cancer. *Cancer Immunology Research*, *7*(5), 784–796. https://doi.org/10.1158/2326-6066.CIR-18-0517

Xiao, S., Yosef, N., Yang, J., Wang, Y., Zhou, L., Zhu, C., Wu, C., Baloglu, E., Schmidt, D., Ramesh, R., Lobera, M., Sundrud, M. S., Tsai, P. Y., Xiang, Z., Wang, J., Xu, Y., Lin, X., Kretschmer, K., Rahl, P. B., … Kuchroo, V. K. (2014). Small-Molecule RORγt Antagonists Inhibit T Helper 17 Cell Transcriptional Network by Divergent Mechanisms. *Immunity*, *40*(4), 477–489. https://doi.org/10.1016/J.IMMUNI.2014.04.004

Zheng, G. X. Y., Terry, J. M., Belgrader, P., Ryvkin, P., Bent, Z. W., Wilson, R., Ziraldo, S. B., Wheeler, T. D., McDermott, G. P., Zhu, J., Gregory, M. T., Shuga, J., Montesclaros, L., Underwood, J. G., Masquelier, D. A., Nishimura, S. Y., Schnall-Levin, M., Wyatt, P. W., Hindson, C. M., … Bielas, J. H. (2017). Massively parallel digital transcriptional profiling of single cells. *Nature Communications*, *8*. https://doi.org/10.1038/NCOMMS14049

Zheng, Y., Collins, S. L., Lutz, M. A., Allen, A. N., Kole, T. P., Zarek, P. E., & Powell, J. D. (2007). A Role for Mammalian Target of Rapamycin in Regulating T Cell Activation versus Anergy. *The Journal of Immunology*, *178*(4), 2163–2170. https://doi.org/10.4049/JIMMUNOL.178.4.2163